

2009

Design, fabrication, and operation of two broadband force balance seismometers

Andrew Weber

Louisiana State University and Agricultural and Mechanical College, aweber4@tigers.lsu.edu

Follow this and additional works at: https://digitalcommons.lsu.edu/gradschool_theses



Part of the [Physical Sciences and Mathematics Commons](#)

Recommended Citation

Weber, Andrew, "Design, fabrication, and operation of two broadband force balance seismometers" (2009). *LSU Master's Theses*. 164.
https://digitalcommons.lsu.edu/gradschool_theses/164

This Thesis is brought to you for free and open access by the Graduate School at LSU Digital Commons. It has been accepted for inclusion in LSU Master's Theses by an authorized graduate school editor of LSU Digital Commons. For more information, please contact gradetd@lsu.edu.

DESIGN, FABRICATION, AND OPERATION OF TWO BROADBAND
FORCE BALANCE SEISMOMETERS

A Thesis

Submitted to the Graduate Faculty of the
Louisiana State University and
Agricultural and Mechanical College
in partial fulfillment of the
requirements for the degree of
Master of Science

in

The Department of Physics and Astronomy

by
Andrew Weber
B.S., University of Maryland, 2002
December, 2009

ACKNOWLEDGMENTS

I would like to thank my thesis director Professor Warren Johnson for all the help and support during the years I have attended LSU. It was his research group in particular that lead me to attend LSU for graduate studies. I would also like to thank my committee members Professor Gabriela González and Professor Juana Moreno for their extra time they gave during this process.

During the development of this project I received invaluable help and advice from the LSU Machine Shop and the Electronics Shop in the Department of Physics and Astronomy. From the Electronics Shop, I thank Brad Ellision, Randy Gould, and Douglas Smith for help with electronics and LabVIEW. For machining, advice, and materials, I extend enormous thanks to George Gascon, Donnie Olano, and Vincent Vaughn. In the Department of Physics and Astronomy office I would like to thank Arnell for timely reminders of approaching deadlines, Rachel for her assistance in purchasing, and Beverly for her friendly help with scheduling.

Throughout my academic years I have received advice, mentorship, encouragement, and inspiration from many people, without which I would not be here. In particular, I would like to thank Professor Bill Hamilton, Professor Ho Jung Paik, Dr. Vol Moody, and Professor Laszlo Takacs. In this category too I will add thanks to an old boss, Mr Quentin Ellis. By lending me a single book, it was he that started the chain of events that would ultimately lead me to where I am today.

I also thank Andrés Rodríguez for his strong encouragement during this project. Others that have facilitated my research include my current boss, Dr. Amitava Roy for his

flexibility and understanding and my colleague Varshni Singh for use of the lapping machine.

Last but by no measure least, I deeply thank my all of my family for their love, support, and encouragement. I thank my loving wife Jessica who pushes me hard by example. I thank her endlessly for enduring periods of single parenthood for the bulk of my writing. I thank my parents, Ronald and Virginia, my brother John Paul, and my grandparents Rex & Dorothy and John & Turelda for providing life-long inspiration and for shaping the character I am today.

This acknowledgment, though not all inclusive, represent some of the most influential people I have come to meet. I am humbled by their collective support, past and present.

TABLE OF CONTENTS

ACKNOWLEDGEMENTS.....	ii
ABSTRACT.....	vi
1. INTRODUCTION	1
1.1 Ground Motion.....	1
1.1.1 Sources of Ground Motion.....	1
1.1.2 Types of Ground Motion.....	2
1.2 Detection Methods	3
1.3 Motivation.....	6
1.4 Project Objective.....	7
1.5 Overview of Thesis.....	8
2. HARDWARE DESIGN	9
2.1 Component Description.....	10
2.2 Alignment of the Proof Mass.....	15
2.3 Proof mass restraint and flex pivot installation.....	15
3. ELECTRONIC DESIGN	17
3.1 Equal Arm Ratio Transformer.....	17
3.2 Capacitors	19
3.3 Phase Sensitive Detector	20
3.4 Data Acquisition Module	22
3.5 Unity Gain Power Amplifier	22
3.6 Linear Voice Coil Actuator	23
3.7 Wiring.....	23
4. FEEDBACK.....	25
4.1 Mechanics.....	25
4.2 Open loop Transfer Function	27
4.3 PID Controller	28
4.4 Closed Loop Transfer Function	29
4.5 PID Tuning.....	30
4.6 Idealized Model Description.....	31
4.7 Control Software.....	36
5. OPERATION.....	38
5.1 Tuning Procedure.....	38
5.2 Step Response	40

6. CONCLUSION	43
6.1 Recommendations for Further Development	43
REFERENCES.....	45
APPENDICES	
A. Mechanical Drawings	48
B. Seismometer_control.vi Block Diagram	64
C. Seismometer_control.vi User Interface.....	65
VITA	66

ABSTRACT

The measurement of ground motion is important for a wide range of fields. In physics, advanced experiments can involve precise positioning of components. In civil engineering, engineers need to know the characteristics of ground motion to better design large scale structures, and the study of ground motion from distant earth quakes help geologists understand the structure and dynamics of the earth.

Each application requires instruments of different specifications. In this thesis I describe the design, fabrication, assembly, and operation of two broad band force balance seismometers and the associated control software. The design, control elements, and methods used in this project can be extended to other applications where specific criteria are needed in the development of custom seismic sensors.

A proportional, integral, and derivative (PID) control scheme was written for the negative feedback loop. Along with the control software, I include a user interface to control the feedback and assist in loop tuning. Closed loop operation of each seismometer was successfully accomplished and the step responses were compared to the step response of an ideal model of the seismometers developed in software. Three parameters are useful in the description of a step response: the settling time, overshoot, and deadtime. The ideal model step response has a settling time of 0.09 seconds and an overshoot of less than 30%. The seismometers exhibit settling times of 1 second and 0.5 seconds and overshoots of 20% and 10%. The ideal model does not exhibit a deadtime but the actual seismometer deadtime was just 30 ms.

1. INTRODUCTION

1.1 Ground Motion

Ground motion is a rich field of study, offering information about the structure of the earth's inner and outer core, offering the location of hydrocarbon deposits below the earth's surface, and even providing verification of a comprehensive nuclear test ban treaty [1]. Instruments to measure ground motion are designed to measure translation and even rotation often simultaneously and in multiple directions. The motion can be quite complex with frequencies ranging over many orders of magnitude and varying with the source.

1.1.1 SOURCES OF GROUND MOTION

In Greek mythology, Poseidon was the "Earth-Shaker," god of earthquakes. When upset, Poseidon would strike the ground with his trident causing the earth to tremor. Today, we know that movement in the earth is caused by several terrestrial sources.

Earthquakes are probably the best known sources of ground motion. During an earthquake, a sudden release of energy from the hypocenter, or the location of the fault rupture within the ground, causes ground motion. The National Earthquake Information Center estimates that each year there are several million earthquakes. Most earthquakes are minor and decrease in frequency of occurrence with increasing magnitude. Sensitive seismometers can detect moderate earthquakes anywhere in the world almost daily.

Anthropogenic activities are another significant cause of ground motion. This "cultural noise" includes automobile traffic, air traffic, mining activities, logging, and petroleum exploration. Cultural noise is often of lower energy and the intensity of cultural noise

decreases quickly at larger distances from the source. Cultural noise is usually found at higher frequency mainly above a few Hz.

Other natural sources of ground motion include meteor impacts, volcanic activity, ocean waves, storms, and winds. The period of ground motion from these sources varies significantly. Oceanic noise, often referred to as microseisms, is one of the most prevalent sources and can be detected all over the world. This widespread and persistent noise is observed to have periods ranging from 4 and 14 seconds. Even the ringing of earth's normal modes which have a period of approximately 100 seconds is detectable with sensitive instruments.

1.1.2 TYPES OF GROUND MOTION

It is increasingly more important for engineers to better understand ground motion as larger structures such as buildings, bridges, and storage tanks with lower resonant frequencies are built [2]. These structures must be safely constructed to withstand the omnipresent motions of the ground. In addition to large-scale structures, characterizing ground motion is also of importance to sensitive scientific experiments requiring precise positioning of equipment [3, 4] [4]. The motion of the ground at any location is very complicated, however there are two basic types of ground motion – body waves and surface waves.

Body waves travel in the earth's interior and are comprised of two types. The first type is called P wave, or primary wave because it is usually the first type of wave to be detected from an event. P waves are higher velocity compression waves that travel through the earth's interior. Like sound waves, P waves act to compress and dilate the earth longitudinally in the direction of propagation. S waves, or secondary waves, have lower

velocity and are usually detected after the initial P waves. S waves are transverse and displace the ground perpendicular to the direction of propagation.

Surface waves occur on the earth's surface and are also comprised of two types.

Rayleigh waves are surface undulations where particle motion is elliptical in the plane made by the direction of propagation and the surface normal. The second type of surface wave displaces the ground in the surface plane perpendicular to the direction of propagation. Although Rayleigh and Love waves travel slower than body waves, they usually have larger amplitudes than S and P type waves.

1.2 Detection Methods

The first instrument known to record ground motion was built by Zhang Heng of China's Han dynasty in 132 CE. The instrument, called Houfeng Didong Yi, was a mechanical device resembling a large urn with eight ornate dragon heads placed 45° apart on the outside wall. Ground motion disturbed a pendulum inside the urn. When disturbed, the pendulum activated levers which released a brass ball from within one of the dragon's mouths depositing the ball inside a cup below. The principal direction of the disturbance could be determined based on which dragon released the ball.

Modern seismometers are much more sensitive and use electronic methods to sense, record, and even control the position of the proof mass. The mechanical design often incorporates a proof mass as a harmonic oscillator with near infinite period. The proof mass then approximates an inertial mass and remains stationary with respect to inertial space as the seismometer housing moves with the ground. To achieve long periods in confined spaces, designers incorporate tilted ridged pendulums, inverted pendulums, leaf springs, zero length springs, and other mechanical methods[5].

One of the simplest methods of detecting relative motion between the proof mass and the seismometer housing involves measuring the current induced by the relative motion of a conductive coil and a magnet. In this voice coil transducer, the magnet, usually mounted to the instrument housing, generates a current in the coil. The measured voltage across a resistor in series with the coil is proportional to the velocity. This is the principle of passive instruments such as the geophone. At low frequencies, currents generated in the coil are too small to measure so typically this method is reserved for a narrower frequency band above 1Hz.

To measure lower frequency ground motion, a modulation scheme is employed whereby a carrier frequency is modulated by the motion of the proof mass. The modulated carrier frequency produces a voltage signal on a half bridge circuit that is proportional to the displacement. Both inductive and capacitive methods are realized for sensor design.

Inductive transducers use a linear variable differential transformer (LVDT) to modulate the carrier frequency. In this configuration, the transformer coils are mounted to the seismometer housing and a magnet is attached to the proof mass. The magnet changes the inductance of the coils and a voltage is produced that is proportional to the displacement. The advantage of this configuration is that no electrical connection to the proof mass is required. The disadvantage, however, lies in the Barkhausen noise of the ferromagnetic material whereby the magnetic domains can spontaneously change size or orientation.

Capacitive transducers modulate the carrier frequency by changing the space between capacitors. The proof mass lies between two capacitor surfaces which are fixed to the instrument housing. In a linear variable differential capacitor (LVDC) design, the motion of

the proof mass changes the capacitance differentially. Unlike the voice coil transducer, the voltage generated at the half-bridge, or Blumlein Bridge (Figure 1-1), is proportional to the displacement of the proof mass and is better suited for measuring lower frequency motion. This design requires an electrical connection to the proof mass but does not suffer from magnetic noise. If designed carefully, it can be a hundred times more sensitive than the LVDT [5] and is the basis of the seismometer electrical design described in Chapter 3 of this thesis.

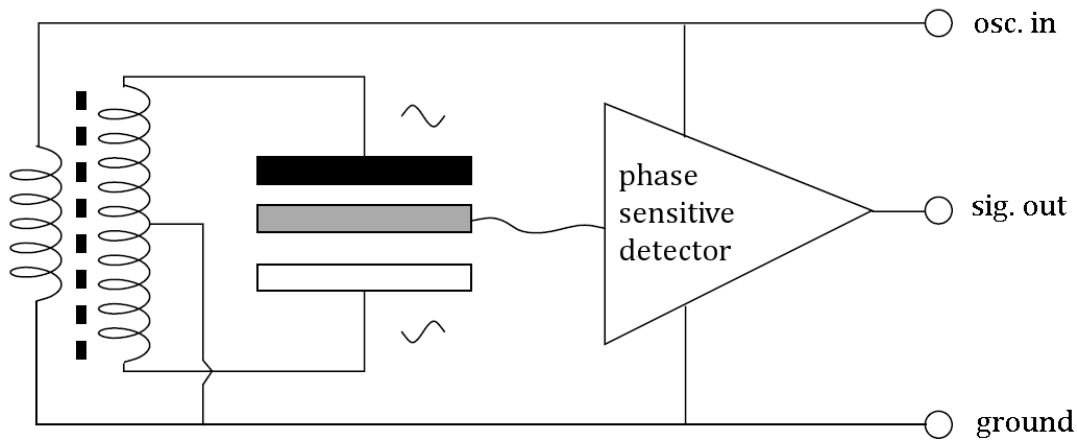


Figure 1-1: In a Blumlein bridge, the outer capacitors receive an AC voltage signal 180 deg out of phase between the plates. The output from the phase sensitive detector is DC and proportional to displacement. Adapted from [5]

Force balance seismometers typically use a transduction scheme described above but also use a feedback loop to control or 'balance' the position of the proof mass using a force actuator. The actuator applies a force on the proof mass that is proportional to the ground acceleration. The proof mass stays fixed relative to the seismometer housing and the feedback signal is recorded. There are several advantages with the force balance technique. Since the mass does not move far from equilibrium, the system is less susceptible to the mechanical limitations of the spring or suspension. The output signal is linear over a wider range of motion since both the variable differential transducer and the

force actuator are operating over much smaller displacements. Despite a high frequency cutoff from the inherent delay in the feedback loop, the force balance principle is used in nearly all modern broadband seismometers operating from .01Hz to 10Hz.

1.3 Motivation

The Laser Interferometer Gravitational wave Observatory (LIGO) in Livingston Parish, is the largest physics research facility in Louisiana. Its purpose is to discover and then observe gravitational waves from various astrophysical sources. Optical components, such as mirrors, used in the interferometer must be isolated from the motion of the ground. Reducing the seismic motion that gets through its vibration isolation system is an important technical problem that must be solved. One of the primary methods under development is "active isolation", where the ground motion is sensed by an array of seismometers, and opposing forces are applied to the suspension in an attempt to make the net force on the test masses go to zero [3, 6]. This problem is most acute at low frequencies from 0.01 to 0.20 Hz. Sensitive, low noise commercial seismometers to measure translation exist but angular or "tip-tilt" seismometers with the same sensitivity and low noise are not commercially available. The non-existence of highly sensitive angular seismometers at lower frequencies is currently a major limit to the performance of these active isolation systems. As a result, invention of such instruments is becoming increasingly important for LIGO.

This thesis is motivated by the need for low frequency angular seismometers. There have been a few attempts to develop angular seismometers over the years[7-9] but the sensitivity requirements for LIGO at low frequencies have not been met because of mechanical resonances and unexpectedly narrow band width. This is perhaps due in part

to $1/f$ noise in the optical sensor or because of insufficient attention to thermal drifts and translational-rotational cross couplings.

Instead of tackling this problem head on, it was decided to make a horizontal seismometer that could test the new technology proposed to solve the problems exposed by the earlier attempts. The device built here incorporates two new features. The first feature is a very large-area small-gap differential capacitance position sensor. We estimate that it ultimately can be one or two orders of magnitude more sensitive than the shadow sensors and linear variable differential inductors, and is likely to have much lower $1/f$ noise. The second feature is a symmetric design aimed at reducing the effect of thermal drift.

Because horizontal seismometers are better developed than angular seismometers, we can make direct comparisons to commercial instruments, and hopefully verify the performance of our design elements. The design elements developed here can then be modified for use in angular seismometers leading to the desired sensitivity levels and noise requirements at low frequencies.

1.4 Project Objective

The objective of this research is to design, fabricate, and demonstrate the operation of two broadband force balance seismometers. Free from design constraints of commercialized seismometers or custom-built seismometers for specific applications, the seismometers designed here could be made larger in size and mass. Larger capacitor plates and a heavier proof mass leads to longer natural periods and increased sensitivity. The electronics could also be removed from the devices leading to the possibility of vacuum operation to further increase sensitivity. Though the seismometers described in this thesis measure ground motion in one direction, the technology demonstrated in this project can

also be applied to the construction multi-dimensional seismometers or tip-tilt rotational sensors that may have practical applications in active isolation systems [3] [10] [11]. The custom fabrication of seismic sensors allows for special consideration to the operational environment and required specifications of the project. Such “purpose built” seismometers are often the only solution for unique applications.

1.5 Overview of Thesis

In Chapter Two I discuss the motives for hardware design including, symmetry, mass distribution, and loads. Each component of the seismometer is discussed and a process for assembly is described. In this chapter I also describe restraining the proof mass should the seismometers be moved.

Chapter Three focuses on the electrical system including design considerations, heat loads, and lock-in amplification. Here, each component of the electrical system is described.

In Chapter Four I discuss feedback principals that are applicable to seismic instruments and theoretical performance of the feedback system implemented in this project. This chapter includes a performance description of a seismometer modeled in software and finishes with an overview of the control program.

In Chapter Five I explain the tuning and closed loop operation of the seismometers and show results for step response. The results are then compared to the closed loop response of the model created in software.

Chapter Six presents a summary of the project and further improvements to realize greater sensitivity and further characterize the performance.

2. HARDWARE DESIGN

This thesis describes the design, construction, and operation of two identical, broadband, force balance, horizontal seismometers. Sometimes I will refer to a single seismometer but it should be understood that the reference applies to both seismometers unless otherwise noted. The basic design of the seismometers described in this thesis is that of the horizontal “garden gate” type in which the proof mass swings, or rotates, horizontally about vertical axis. The motivation for the hardware design stems from the criteria for which they were constructed. Two identical seismometers were constructed mainly for the purpose of characterizing their performance since two identical seismometers operating simultaneously and in different configurations can yield additional information about the motion of the ground. Each seismometer was designed such that air currents would be reduced or eliminated and their effect on the proof mass minimized. The seismometers were also designed with a high degree of symmetry to mitigate the effects of thermal expansion of components. The use of ferrous material was avoided throughout the instruments to prevent parasitic forces on the swing arm actuator. As a result, all mounting hardware is brass. The mass distribution was chosen carefully such that forces on the flex pivots were minimal while keeping the proof mass large. These design characteristics were chosen with the design goal of a large bandwidth between .01 Hz to 10Hz operating near the USGS Low Noise Model [12].

Three-dimensional models for each component of the seismometers were created in the computer-aided design software program Pro/ENGINEER 2000i. The design specifications of each component were created to not only satisfy the seismometer design criteria but also to facilitate standard machining practices. Each of the three-dimensional renderings

were assembled in software to create a 3D virtual model of the complete seismometer. After the model dimensions and clearances were verified, each individual component was flattened to a set of two-dimensional mechanical drawings to aid in the machining of the components. The drawings, along with a 3D rendering of the assembly are included in Appendix A.

Both staff machinists at the LSU Machine Shop and I, in the Department of Physics and Astronomy student machine shop, machined the parts for the seismometers. After machining, the parts were cleaned in a method adapted from B.S. Halliday for rough vacuum components [13]. After the parts were swabbed or immersed in acetone, then ethanol, and finally water, the final assembly was made.

2.1 Component Description

The base plate upon which the components of the seismometers are placed was fabricated from a single 1.5 inch thick aluminum plate. On the bottom side of the plate, three adjustable brass legs are located 120° apart. Once the plate is level, the leg just under the axis of rotation can be used to adjust the angle α between the axis of rotation and vertical. The legs are threaded # $\frac{1}{2}$ "-28 and the distance from the back leg to the axis defined by the front two legs is 9.563". One complete revolution of the leg will change α by 0.214 degrees. This adjustment is used to alter the period of the swing arm. For small amplitudes of a simple inclined pendulum, this relation is given by

$$T = 2\pi \sqrt{\frac{l}{g \sin \alpha}}, \quad (2.1)$$

where g is the acceleration due to gravity and l is the distance from the axis of rotation to the mass. Each seismometer includes a Starrett # 98, 6 inch, precision ground level.

Each graduation on the main vial indicates a tilt of .005"/foot or 87 arcseconds. The levels also include a coarse cross vial for simultaneous leveling.

The mast sits atop the base plate and suspends the swing arm. The mast, like the capacitor holders discussed later, was designed with three legs for stability. Each of the three legs meet at a central vertical column at the center of the mast between the two flex pivot clamps. The mast was designed to minimize any temperature differential that may exist between the flex pivot clamps should there be a non-zero heat flow from the base plate.

Commercial flex pivots were chosen to attach the mast to the swing arm because they have zero rolling or coulomb friction, zero backlash, low thermal drift, and virtually no hysteresis at low deflection angles[14]. Flex pivots from Riverhawk (catalogue # 6005-800) were chosen to meet the design loads with acceptable safety margins and with the lowest torsional spring rate. Table 2-1 lists the pivot load capacities along with expected loads on the pivot from the seismometer. It should be noted that the loads are assumed to be in tension, not compression. The loads described in Table 2-1 are for radial loads in tension as labeled V_t in Figure 2-1.

Table 2-1 Maximum load data for Riverhawk single flex pivot catalogue # 6005-800 and seismometer load estimates. Riverhawk data adapted from [15]

	Riverhawk Data	Riverhawk Data (MKS)	Seismometer Load Estimates
Axial Load P_a (N)	9.7 lbs	43.1 N	12.8 N
Radial Load V_t (N)	7.4 lbs	32.9 N	13.8 N
Torsional Spring Rate	.0004 $\frac{in-lb}{deg}$	$2.59 \times 10^{-3} \frac{Nm}{radian}$	NA

Load Capacity for compressive loads (V_c) are less than half of those for loads in tension and would not provide a suitable margin of safety. Therefore, careful attention to flex pivot orientation has been made to insure loads are in tension.

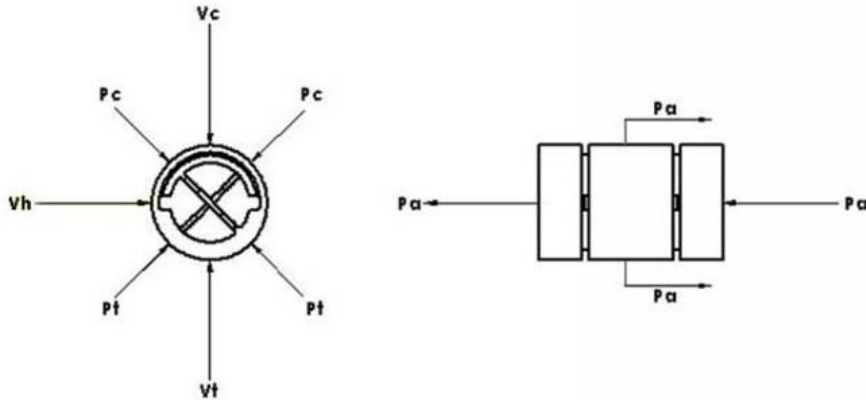


Figure 2-1: Diagram showing loads and load labels for Riverhawk double-ended flex pivots[15].

The swing arm extends from the flex pivots to the proof mass and is allowed to rotate about the flex pivot axis. There were three main criteria for the design of the proof mass – swing arm assembly.

First, the capacitance between the proof mass and the base capacitor should be large. Neglecting fringe effects, this capacitance is calculated to be 220 pF assuming an average spacing of 100 microns.

The second criterion is high mass. Brownian motion of the proof mass is inversely proportional to the mass M and forms the fundamental limit to detection. It is shown [16] that the mechanical noise equivalent acceleration over a bandwidth Δf is given by

$$(\ddot{x})^2_{MNEA} = \frac{4dkT\Delta f}{M^2} = \frac{4kT\omega_0}{MQ} \quad (2.2)$$

where kT is the equipartition energy, d is the damping coefficient, Q is the quality factor, and ω_0 is the natural frequency. The mass was made large at 1.1 kg and if we

assume $Q = 100$ and $\Delta f = 1 \text{ Hz}$, then $(\ddot{x})_{MNEA}^2 \approx 7 \times 10^{-12} \text{ m/s}^2$ which is two orders of magnitude lower than the USGS New Low Noise Model.

The third criterion is low moment of inertia about the center of mass to reduce the force on the flex pivots as the ground accelerates. To accomplish this, aluminum was chosen as the material and lightening holes were drilled along the swing arm to remove material away from the center of mass. Mass properties of the swing arm including the proof mass are highlighted in Table 2-2.

Table 2-2: Mass properties of the swing arm

Mass of Swing Arm	Distance of CM from pivot	Moment of Inertia about CM I_{zz}	Moment of Inertia about pivot I_{zz}
1.10 kg	14.6 cm	0.0480 Nm^2	0.279 Nm^2

The copper proof mass is bonded to, and electrically insulated from, the arm capacitor holder with Stycast 2850FT. This two-component epoxy encapsulant was chosen for its relatively high elastic modulus and high thermal conductivity. After the proof mass was bonded to the arm capacitor holder, the copper surface was fly cut to be flat and coplanar with the aluminum arm capacitor holder. After fly cutting, the capacitor surfaces of the proof mass were wet polished with a lapping machine from Hyprez Lapping Systems first starting with a 600 grit, then finally with a 800/2400 grit silicon carbide abrasive disk.

The base capacitor holders are rigidly mounted to the base plate on each side of the swing arm with a single $\frac{1}{2}$ " - 13 brass bolt for easy alignment (see 2.2 Alignment and Constraint). Like the proof mass, the base capacitors were electrically insulated from, and bonded to, the aluminum capacitor holders using Stycast 2850FT, fly cut, and polished using the same methods. During the machining, care was taken to ensure that the capacitor

sensing faces were perpendicular to the plane made by the bottom three feet. The surfaces meet this criteria to better than 1 part in 3000.

Next to the base capacitor holder lies the magnet holder. The magnet holder is designed to hold and position the magnet part of the linear voice coil actuator (LVCA). The LVCA provides the restoring force needed to keep the swing arm fixed relative to the base capacitor holders during closed loop operation. The oversized mounting hole on the magnet holder aids the alignment of the magnet with the voice coil mounted on the swing arm.

The lifter, located under the swing arm, is designed to relieve the load from the flex pivots during relocation and storage. The lifter consists of three main parts: the lifter body, the load screw, and the action screw. The action screw has a pitch of 32 tpi and controls the contact pressure on the swing arm while the load screw makes contact with the swing arm. The lifter body is designed to be a lever with an arm ratio of approximately 5:1. One complete revolution of the action screw will raise or lower the load screw by about .0063 inches or 0.16mm.

Each seismometer has a bulkhead mounted brass pumpout flange designed to be compatible with ISO KF-NW25 type fittings. This pumpout port allows the regulation of pressure inside the seismometer vessel.

Finally, each seismometer is enclosed in a custom-made 12" inner diameter acrylic bell jar from Nevada Vacuum. During normal operation, the bell jars eliminate environmental air currents and help to reduce temperature fluctuations. The bell jars are also vacuum compatible.

2.2 Alignment of the Proof Mass

The base capacitors were specifically designed with large mounting holes to aid in the alignment process. The single large hole in each of the base capacitors allow for easy rotation and translation. Oversized holes were also made in the swing arm to allow for rotation.

The first step when aligning the proof mass for the first time was to insert pins in place of the flex pivots to prevent damage. The two screws that hold the proof mass to the swing arm were then loosened but not removed. Next, the bolts that mount the outer capacitors were loosened. This allowed the proof mass to rotate slightly about a horizontal axis and the base capacitors to rotate about the vertical axis. With paper or film between the capacitor surfaces for protection, the two outer capacitors were pressed tightly against the central capacitor insuring parallel surfaces. Once the central capacitor was parallel with the outer capacitors, the mounting screws and bolts were tightened. The gaps between the capacitors were set by selecting the appropriate thickness paper or film.

2.3 Proof mass restraint and flex pivot installation.

To install the flex pivots, the proof mass was secured. With the paper or film still in place, the action screw on the lifter was loosened. Next, the load screw was unscrewed until it made contact with the swing arm. Then the action screw was tightened until the head of the load screw made contact with the swing arm. The action screw was then turned an additional $\frac{3}{4}$ revolution to apply pressure to the bottom of the swing arm. With the proof mass and swing arm secured, the brass pins were replaced by the flex pivots. It should be noted that the flex pivots have *opposite* orientations; the bottom flex pivot is

rotated 180° from the top flex pivot such that the loads are in tension for both pivots. The tension vector V_t in figure 2-1 points toward the capacitors for the top flex pivot.

3. ELECTRONIC DESIGN

The design of the seismometers incorporates a three-plate capacitive displacement transducer operating on the force balance feedback principle as first discussed in Section 1.2 of this thesis. The electrical system includes the equal arm ratio transformer, the central capacitor plate, the two base capacitor plates, the lock-in amplifier, the data acquisition module, the unity gain power amplifier, the linear actuator coil, and associated connectors and wiring.

3.1 Equal Arm Ratio Transformer

The design of the equal arm ratio transformer and bridge is adapted from the seminal paper on capacitive micrometers by Jones and Richards[17]. As seen in section 1.2 above, a modulation signal is sent from the lock-in amplifier to the equal arm ratio transformer. The outputs, $v_1 \pm$ of the transformer are 180° out of phase and are fed to the base capacitor plates. If the voltage across the secondary coils in the transformer is $2v_1 \sin \omega t$, then the current from the center capacitor to ground is $\Delta C v_1 \omega \cos \omega t$ where ΔC is $C_1 - C_2$ as described by Jones and Richards. This relation highlights the importance of operating the seismometer with a large capacitance and a large carrier frequency ω , however a limit on the carrier frequency is imposed by the stray reactances. Jones and Richards describe the condition for a balanced bridge as

$$\frac{C_1}{C_2} = 1 + L_B(C_2 + C_B)\omega^2 + L_A(C_1 + C_A)\omega^2 + \frac{R_E}{R_A} - \frac{R_F}{R_B} + \frac{\delta v_1}{v_1} . \quad (3.1)$$

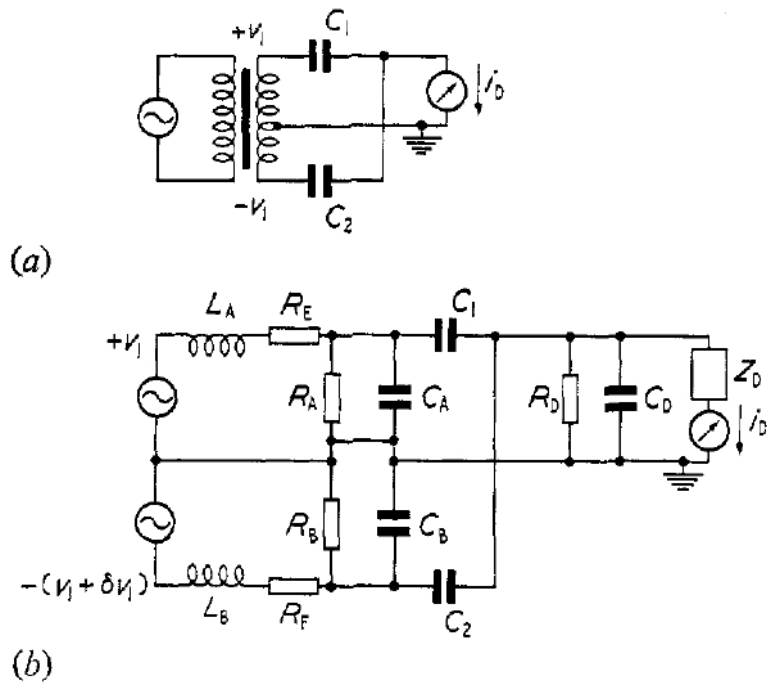


Figure 3-1: (a) Transformer ratio bridge; (b) equivalent circuit [17]

For the seismometers, assuming L_A and L_B are $1 \mu\text{H}$ each, total capacitance in each term of 500 pF , and a modulation frequency of 20kHz , a change in either L_A or L_B by one part in 100 is equivalent to a change in C_1/C_2 by 10^{-7} . Though a change in the secondary winding inductance of 1% is not likely, it illustrates the importance of secure transformer windings and using a reasonable modulation frequency.

The transformer primary winding was wound with 50 turns of enameled 28 AWG (.0126" dia.) copper wire on a ferrite pot core. The grounded secondary winding was made with the same copper wire with 20 turns. Between the two windings is an electrostatic shield of grounded copper foil. The transformer was placed inside a sealed metal electrical box with an input BNC connector to the primary winding. The two ends of the secondary

winding lead to a twinax connector with two inner conductors and a grounded sheath. The center tap of the secondary winding and the center foil was attached to the metal box and connector bodies.

3.2 Capacitors

The two base capacitors and the central capacitor have a diameter of 5.68 cm. The spacing between the central proof mass capacitor and the base capacitors is adjustable but the spacing for the initial configuration is 100 μm between each plate. With a stable and robust feedback loop in place, the spacing can be reduced. With a spacing of 100 μm and ignoring the extra capacitance from fringe fields, the calculated capacitance between the center capacitor and the base capacitor is 220 pF. A change in the gap between the capacitors of 1 nm from the balanced condition changes the capacitance by 4.5 fF. This corresponds to a change in the quantity C_1/C_2 , of 2×10^{-5} .

A parallel plate capacitor experiences an electrostatic force between the plates that is proportional to the square of the driving voltage and inversely proportional to the square of the distance between the plates. The advantage of a differential capacitance bridge of this design is that the central proof mass capacitor will have zero electrostatic force when the system is balanced. There does exist a small non-restoring force when the seismic mass is displaced from center. The force on the displaced seismic mass is given by[18]

$$F_e = \frac{A\epsilon_r\epsilon_0(2v_1)^2}{2d_0} \left(\frac{1}{1 - \frac{x}{d_0}} - \frac{1}{1 + \frac{x}{d_0}} \right), \quad (3.2)$$

where A is the area of the capacitor plate, d_0 is the gap across the balanced capacitor, x is the displacement, and ϵ_r and ϵ_0 are the relative and free space permittivities respectively.

Assuming a displacement of 1 μm and an rms voltage v_1 of 1 V, the force is about 0.1 μN .

Even with very large excursions, the force F_e on the proof mass is significantly less than the force that can be supplied by the feedback coil. Displacements of this size are not expected during normal closed loop operation and thus F_e will not be considered further.

3.3 Phase Sensitive Detector

In a phase sensitive detection scheme, an experiment is excited with a reference signal, typically a sine wave from a function generator. The output signal from an experiment includes the reference signal and some modulation related to the quantity to be measured. A phase sensitive detector (PSD) then multiplies the reference signal from the oscillator, $V_{ref}\sin(\omega_{ref}t + \theta_{ref})$, and the modulated signal from the experiment, $V_{sig}\sin(\omega_{sig}t + \theta_{sig})$. The unfiltered output from the PSD is then

$$V_{PSD} = V_{sig}V_{ref} \sin(\omega_{sig}t + \theta_{sig})\sin(\omega_{ref}t + \theta_{ref}) . \quad (3.3)$$

Using the products as sums identity, this can be rewritten as

$$V_{PSD} = \frac{1}{2}V_{sig}V_{ref} \cos((\omega_{sig}t - \omega_{ref}t) + \theta_{sig} - \theta_{ref}) - \frac{1}{2}V_{sig}V_{ref} \cos((\omega_{sig}t + \omega_{ref}t) + \theta_{sig} + \theta_{ref}) . \quad (3.4)$$

There are two signals here, one at the difference frequency between the reference signal and the experiment signal and the other at the sum frequency. V_{psd} is then low pass filtered, leaving only the phase contribution. The low pass filtered output from the PSD is then

$$V_x = \frac{1}{2}V_{sig}V_{ref} \cos(\theta_{sig} - \theta_{ref}) . \quad (3.5)$$

The output is proportional to V_{sig} and depends on the phase difference between the reference and the signal from the experiment[19]. To remove the phase difference all

together, some lock-in amplifiers have a second PSD that multiplies the signal from the experiment, $V_{sig} \sin(\omega_{sig} t + \theta_{sig})$ by the reference signal shifted 90° . The filtered output is then

$$V_y = \frac{1}{2} V_{sig} V_{ref} \sin(\theta_{sig} - \theta_{ref}). \quad (3.6)$$

V_y in equation 3.6 is the quadrature and V_x in equation 3.5 is called the in-phase component. Together, the phase independent magnitude of the signals can be found

$$R = \sqrt{(V_x^2 + V_y^2)} = \frac{1}{\sqrt{2}} V_{sig} V_{ref} \quad (3.7)$$

Typical detection schemes not involving phase sensitive detection measure not only the signal of interest but also broadband white noise, which can be many orders of magnitude larger than the signal of interest. The addition of a high Q bandpass filter can help reduce the noise but the passband can still be too large.

Phase sensitive detectors measure the signal in a very narrow frequency band, eliminating noise outside the frequency range. Since the frequency of the reference signal can be adjusted, the signal can be moved into a less noisy part of the spectrum to reduce $1/f$ noise and avoid line frequency interference.

For the measurements described in this thesis, a Stanford Research Systems model SR830 lock-in amplifier is used for phase sensitive detection. The reference signal used here is generated by a crystal oscillator inside the lock-in and has a maximum RMS voltage of 5V and is frequency adjustable from 1 mHz to 102 kHz. If a larger voltage is required to drive the experiment, a separate function generator can be used. The lock-in uses a phase-lock-loop (PLL) to lock the frequency and phase of the function generator to reference

signal. Using an external function generator, however, introduces a phase noise of a few millidegrees which shows up in the in-phase and quadrature measurements[19].

3.4 Data Acquisition Module

Output from the lock-in amplifier is fed to a National Instruments model 6211, 16 bit, m series, multifunctional data acquisition (DAQ) module. The analog signal is digitized and sent to a computer via universal serial bus (USB) for signal processing and recording. As discussed in Section 4.7 below, the control loop is handled in software by the computer. The output signal, in the form of feedback, is sent from the computer to the DAQ then to the linear voice coil actuator. The DAQ has 16 analog inputs and 2 analog outputs with a maximum voltage range of ± 10 V. Each channel can record at 250k samples per second with 16 bit resolution.

3.5 Unity Gain Power Amplifier

The output from the DAQ can swing to ± 10 V but the maximum current from the device is limited to just 2 mA. To drive the voice coil actuator, rated for peak current of 1.2 A or approximately 5.75 W, a National Semiconductor model LM675T power operational amplifier at unity gain was chosen to drive the load. The LM675T can supply a maximum current of 3 A and has a thermal protection circuit to protect against overheating [20]. The voltage from the DAQ to the LM675T has been limited to ± 3 V to protect the voice coil actuator.

3.6 Linear Voice Coil Actuator

The non-contacting LVCA consists of two parts: the magnet, mounted to the base, and the voice coil, mounted to the swing arm. The permanent magnet was mounted to the base to reduce the effects of stray magnetic fields on the swing arm. The voice coil mounted to the swing arm is well shielded but adds the necessity for current carrying wires to the swing arm as discussed in section 3.7 below.

Model number LA05-05-000A non-contacting linear voice coil actuators were chosen from BEI Kimco for their performance and compact size. Table 3-1 highlights some important parameters about the LVCA.

Table 3-1 Data from BEI Kimco for linear voice coil actuator model number LA05-05-000A [21].

Part no.	Peak Force (N)	Continuous Stall Force (N)	Total Stroke (mm)	Actuator Constant ($N/\sqrt{\text{watt}}$)	Force Sensitivity N/Amp
LA05-05-000A	0.7	0.31	1.02	0.289	0.575

3.7 Wiring

Three, twin-conductor, bulkhead mount, feedthrough connectors (Detorionics part # DT07H-8-2PN) are mounted to the base plate – one between the base capacitors and the other two by the mast. One connector supplies both signals for the base capacitors, another connector supplies the current for the voice coil actuator, and the third connector provides the output signal from the proof mass capacitor on a single conductor.

The signal from the transformer is transmitted to the feedthrough near the base capacitors with a twinax cable. Two single coaxial cables run from the base plate

feedthrough to each of the two base capacitor plates with the outside of the coaxial cable grounded to the aluminum structure surrounding the capacitor. Similarly, the signal from the central capacitor is sent by a coaxial cable to a single center conductor on a feedthrough at the mast. The current to the voice coil actuator is carried by a twisted pair of silver plated 28 AWG stranded silicone coated wire soldered to the two inner conductors of the feedthrough.

The coaxial cable from the center proof mass capacitor and the twisted pair from the voice coil are required to cross the swing arm to the mast. At the crossing point between the flex pivots, jumper wires are used to bridge the gap. Small diameter jumper wires were chosen to minimize contribution to the spring constant and reduce mechanical dissipation. In addition all the jumper wires were located such that they cross the axis of rotation to prevent torque from thermal length changes. As an additional safeguard against forces of thermal origin, the jumper wires were soldered so as not to be in tension.

The jumpers for the signal carrying coaxial cable were made with 46 AWG (.0016" dia.) silver plated copper wire. The outer conductor has two jumpers, one above and one below the center conductor to reduce the pickup of electromagnetic noise. The jumpers for the current carrying wires are 36 AWG (.005" dia) and are bare copper. The 36 gauge current carrying wires have a resistance of 16.3 Ω /m and will not dissipate more than .1 W each during the most extreme operation.

4. FEEDBACK

Feedback has been used in seismometer design since the 1960's [22], which allowed seismometers to operate at longer periods and over wider frequency bands. The first of the seismometers to incorporate electronic sensing with feedback was the modified LaCoste-Romberg with electrostatic force feedback[23]. Since that time, electronic sensing and feedback is still used in the most advanced seismometers today[11].

The error signal, in this case a measure of the difference between the desired position of the seismic mass and the actual position of the mass, is used to provide a restoring force on the seismic mass in a negative feedback closed loop control system. The control system implemented here is closed loop with a software-managed PID controller.

4.1 Mechanics

Though the seismometers described in this thesis are operated in a closed loop mode, it will be useful to describe the open loop characteristics briefly before describing the closed loop behavior in section 0 below. An open loop system has no feedback and its output is strictly a response of the input signal.

The equation of motion for the seismometer swing arm is

$$-I\ddot{\theta}_g(t) = I\ddot{\theta}(t) + d\dot{\theta}(t) + (k + k_\alpha)\theta(t), \quad (4.1)$$

where $\ddot{\theta}_g$ is the angular acceleration of the ground, θ is the angular position of the swing arm relative to the seismometer housing, I is the moment of inertia of the swing arm, d is the damping constant, k is the torsional spring rate, and k_α is the addition of the gravitational contribution to the spring constant from the incline angle α . Since the

seismometer measures very small angular displacements and it's more useful to discuss translations, Equation 4.1 can be rewritten to an equivalent translational form

$$-m\ddot{x}_g(t) = m\ddot{x}(t) + d'\dot{x}(t) + k'x(t) , \quad (4.2)$$

where \ddot{x}_g is the ground acceleration, x is the linear position of the center of mass of the swing arm with respect to the seismometer housing, m is the mass, d' is the linear damping, and k' is the spring constant equivalent.

The linear position of the swing arm x , will be taken at the center of mass located at the capacitor plate 14.6 cm from the flex pivot. In this case, m is just the mass of the swing arm. The spring constant can be found from the torsional spring rate by noting that

$$rF = -k\theta \approx -k \frac{x}{r} .$$

Here, r is the distance from the flex pivot to the measurement point x . We see that

$F = -kx/r^2$ and that the spring constant equivalent is $k' = k/r^2$. From the value of k in

Table 2-1, and noting that there are two flex pivots in parallel, k' is found to be 0.243 N/m.

Finally, k_α is just the restoring force of a pendulum modified by the $\sin \alpha$ term. Assuming an angle $\alpha = .05$ degrees or approximately two divisions on the Starrett level, k_α is 0.064 N/m.

The linear spring constant k' will then be taken as 0.31 N/m.

Mechanical damping for the seismometers here is minimal and its most significant source is estimated to be viscous squeeze-film air damping between the capacitor surfaces. The approximation of the damping constant for circular plates at low vibrational frequency is given by [24]

$$d' = \frac{3\mu A^2}{2\pi h^2} , \quad (4.3)$$

where A is the area of the plates, h is the average separation of the plates, and μ is the viscosity of air. If the area of the entire capacitor housing of the swing arm is used and both sides of the plate are considered, the value for d' is roughly 0.0010 Ns/m.

Dividing equation 4.2 by m and rewriting the constant terms we have

$$-\ddot{x}_g(t) = \ddot{x}(t) + 2\epsilon\omega_0\dot{x}(t) + \omega_0^2x(t) . \quad (4.4)$$

The damping ratio is $\epsilon = 0.00086 \ll 1$ so the system is underdamped as expected. The natural period is 23.7seconds.

4.2 Open loop Transfer Function

The transfer function is the ratio of the Laplace transform of the output over the Laplace transform of the input. The Laplace transform has the advantage that the derivative in the time domain corresponds to a multiplication with s in the Laplace domain. Therefore more difficult differential equations can be replaced with easier algebraic equations [25]. The Laplace transform is defined as

$$\mathcal{L}[f(t)] = \int_0^{\infty} f(t)e^{-st} dt = F(s) , \quad (4.5)$$

Where $s = \sigma + i\omega$ is a complex number. The benefit of the Laplace transform exemplified here:

$$\mathcal{L}\left[\frac{d}{dt}f(t)\right] = sF(s) . \quad (4.6)$$

The Laplace transform of equation 4.2 is then

$$-s^2X_g = s^2X(s) + 2\epsilon\omega_0sX(s) + \omega_0^2X(s) , \quad (4.7)$$

and the open loop transfer function with force as the input and position of the proof mass as output is given by

$$T_{OL}(s) = \frac{X(s)}{X_g(s)} = \frac{-s^2}{s^2 + 2\epsilon\omega_0s + \omega_0^2} \quad (4.8)$$

The location of the zeros of the transfer function along with the roots of the denominator, called poles of the characteristic equation, determine the stability of the system. The closed loop stability of the seismometer will be explored in Section 4.5 below.

4.3 PID Controller

In a PID controller, the error signal is multiplied by three gains before it is sent to the seismometer. The error signal in this case is a voltage from the lock-in amplifier. The error signal reads zero volts for the desired center position and a non-zero voltage proportional to its displacement when not centered. In the controller, the error signal is multiplied by each gain, the proportional gain, the integral gain, and the derivative gain. The gains are then summed before being sent to the linear voice coil actuator as a negative feedback signal. If the error signal is represented by $v_e(t)$, then the feedback signal to the voice coil actuator is given by:

$$V_{fb}(t) = K_p v_e(t) + K_i \int_0^t v_e(\tau) d\tau + K_d \frac{d}{dt} v_e(t), \quad (4.9)$$

where K_p , K_i , and K_d are the coefficients for the proportional, integral, and derivative terms respectively.

The proportional gain determines the quickness of the response of the controller. A larger value of K_p will shorten the response time but can add instability and oscillations to the system. The integral coefficient reduces long-term drift but requires overshoot of the

desired position to null the value of the integral term. The derivative coefficient reduces the overshoot of the desired position but may add instability if K_d is large and if there is a high level of noise in the error signal.

4.4 Closed Loop Transfer Function

To formulate the closed loop transfer function, the individual transfer functions of the system components must be taken into account. The transfer function $G(s)$ of the PID controller is

$$G(s) = K_p + \frac{K_i}{s} + K_d s = \frac{K_d s^2 + K_p s + K_i}{s} \quad . \quad (4.10)$$

A Block diagram of the system is shown in Figure 4-1 The transfer function of the lock-in amplifier α , and voice coil actuator β , are described as a simple gains with units of volts/meter and meter/volt respectively. If the gains of the PSD and actuator are taken into account, the full closed loop transfer function of the model loop show in Figure 4-1 can be stated as

$$\frac{X(s)}{X_g(s)} = T_{CL}(s) = \frac{T_{OL}(s)G(s)\beta}{1 + T_{OL}(s)G(s)\alpha\beta} \quad . \quad (4.11)$$

Filling in the terms for $G(s)$ and $T_{OL}(s)$ and simplifying, the closed loop transfer function is

$$T_{CL}(s) = \frac{s^2 K_d \beta + s K_p \beta + K_i \beta}{s^3 + s^2 (K_d \alpha \beta + 2\epsilon \omega_0) + s (K_p \alpha \beta + \omega_0^2) + K_i \alpha \beta} \quad . \quad (4.12)$$

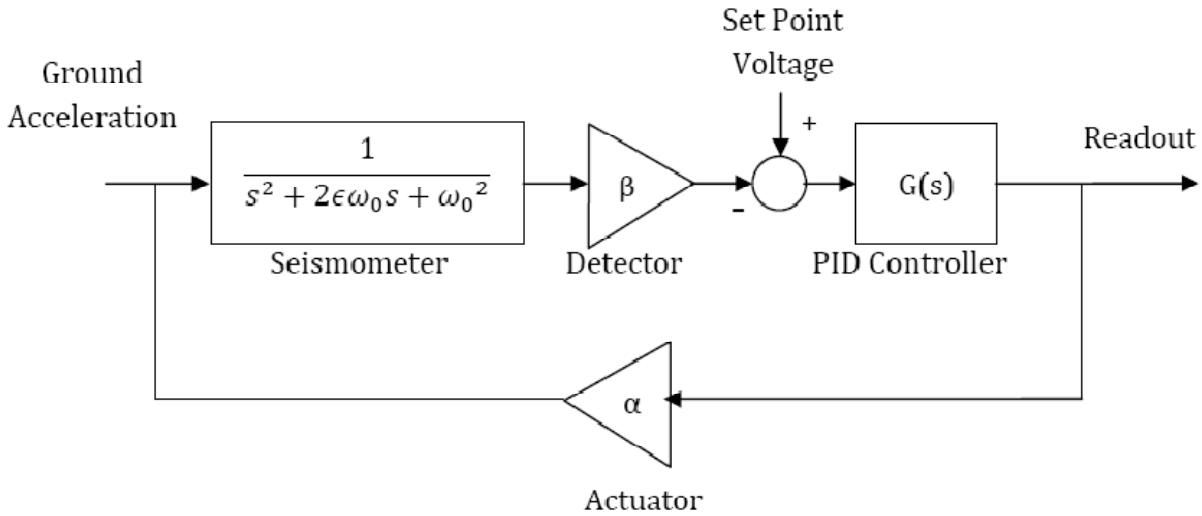


Figure 4-1: Block diagram of the seismometer control loop.

4.5 PID Tuning

Tuning the PID controller involves finding the three coefficients, K_p , K_i , and K_d such that the controller provides the desired output response. There are a few ways to tune the control loop.

The first method for tuning a control system is the trial and error method. If a controller incorporates only a proportional component to the feedback this method can yield satisfactory results. When a PI or a full PID controller is implemented, or when the response time of the system is long, this method may not be practical.

Another method of tuning a PID controller manually was described by Ziegler–Nichols [26]. With the system in closed loop operation, the K_i and K_d terms are set to zero. Next, the K_p term is increased until the process variable, here the voltage from the lock-in amplifier exhibits stable oscillations. The lowest value of K_p for which the system oscillates

is termed the ultimate gain, labeled K_u . The period of oscillation is measured and termed T_u . From these values, the constants K_i and K_d are found from the following relations

$$\begin{aligned}K_p &= 0.6 K_u \\K_i &= 0.5 T_u \\K_d &= 0.125 T_u\end{aligned}\tag{4.13}$$

An open loop method of tuning a controller exists where the process variable is allowed to settle to some nominal value. Then a step change is given to the system while the PV is monitored. From the time it takes for the process variable to respond, referred to as deadtime, and the time it takes the process variable to reach the nominal value, the PID constants can be found. The characteristics of the seismometers described here are not particularly suited for this tuning method therefore details of this method are not provided.

In addition to the manual tuning methods, some software-implemented PID controllers have the capability of autotuning. Autotune methods typically measure the change in the process variable after a step change in the set point variable. From the response, the software determines information such as the deadtime and the time constant needed to optimize the three PID constants.

4.6 Idealized Model Description

To obtain a set of values for K_p , K_i , and K_d , an idealized model of the seismometer and the control loop was developed in the simulation environment Simulink by The MathWorks and integrated with Matlab. A graphical display of the simulation loop is shown in Figure 4-2. Here, the gain β is set to unity and α has been absorbed into the PID constants.

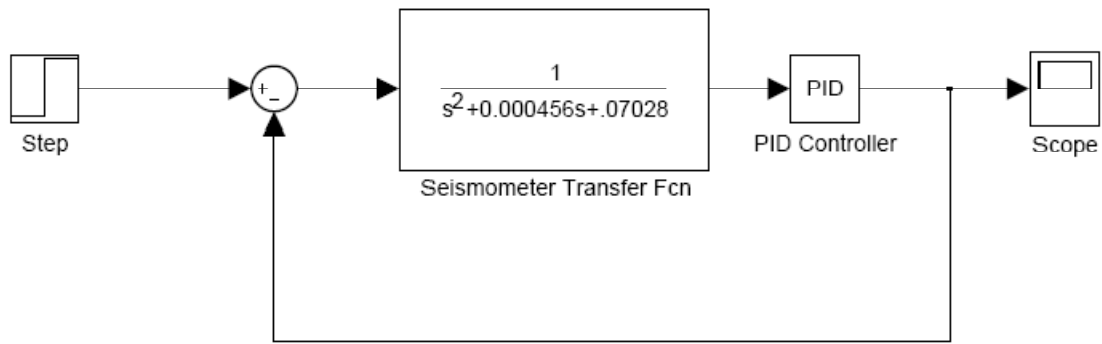


Figure 4-2: Simulink block diagram of the seismometer control loop

The output of the step response can quickly be observed as the parameters are changed. Figure 4-3 shows the step response for the system modeled in Simulink. The PID constants used to generate the step response are listed in Table 4-1 below.

Table 4-1: PID values for the simulated controller

K_p	K_i	K_d
2200	40	52

The response has a settling time (4%) of 0.09 seconds and an overshoot of less than 30%. The overshoot is a consequence of fast rise time and low damping. In other processes where overshoot is unacceptable, it can be controlled by increasing the damping ratio or a combination of decreasing K_i and increasing K_d .

With the constants in Table 4-1, the closed loop transfer function in equation 4-12 can be written as

$$T_{CL}(s) \approx \frac{52s^2 + 2200s + 40}{s^3 + 52s^2 + 2200s + 40} \quad (4.14)$$

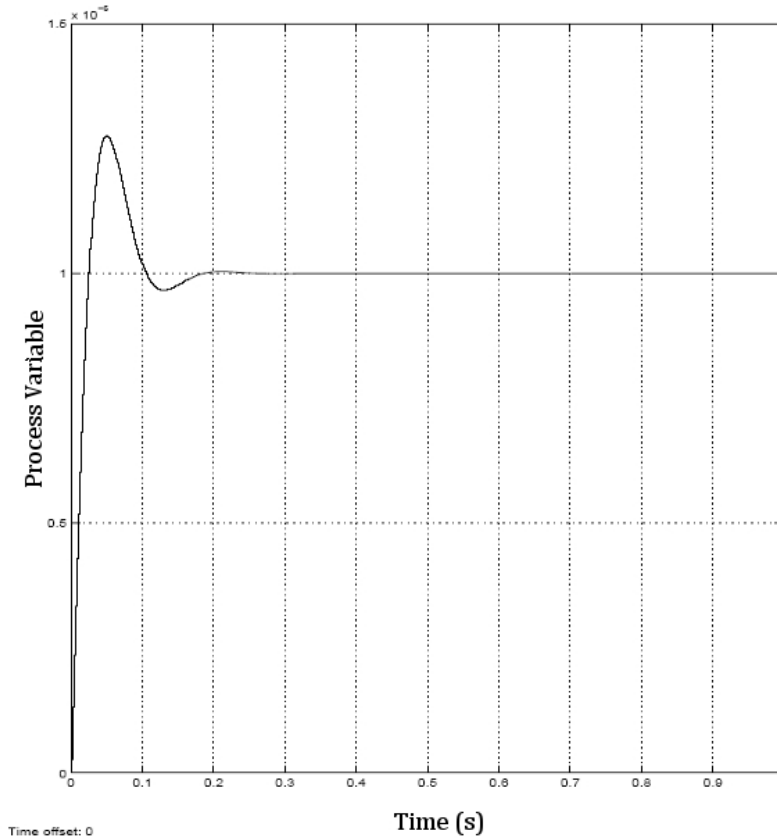


Figure 4-3: Step response of Simulink model

Equation 4.14 is approximate since the denominator has the very small contribution from the $2\epsilon\omega_0$ and ω_0^2 terms. The operation of the feedback loop is dominated by the PID controller.

The zeros of the numerator and the poles of the denominator are listed in Table 4-2.

Table 4-2: Poles and Zeros of the closed loop model transfer function

Zeros (rad/s)	-42.2895	-0.01819
Poles (rad/s)	$-25.9907 \pm -39.0316i$	-0.01819

simple plot of the poles and zeros of the transfer function in the complex – s plane yields a

graphical tool useful in the analysis of the frequency response[27]. Since all the poles are in the left half plane (ie. $\sigma < 0$) the system is stable and will have a bounded output for all bounded inputs. Also as seen in the figure below, a pole and a zero very nearly cancel and thus the system is approximately a second order system. From the pole zero plot, the magnitude of the frequency response at a frequency ω is determined by the ratio of the products of the lengths of the vectors from the pole location to the complex frequency on the $i\omega$ axis to the length of the vector from a zero to the same frequency.

The Bode plot showing the frequency and phase response of the model closed loop transfer function is plotted in Figure 4-5. From the pole zero plot, it can be seen that the magnitude of the frequency response reaches a maximum where the pole makes its closest approach to the imaginary axis. This is confirmed in the frequency response of Figure 4-5 where a peak occurs at near 40 rad/s. The slight resonance at 40 rad/s can be seen on the step response above as quickly decaying oscillations with the same frequency. The 3dB cutoff frequency is about 80 rad/s or roughly 25 Hz.

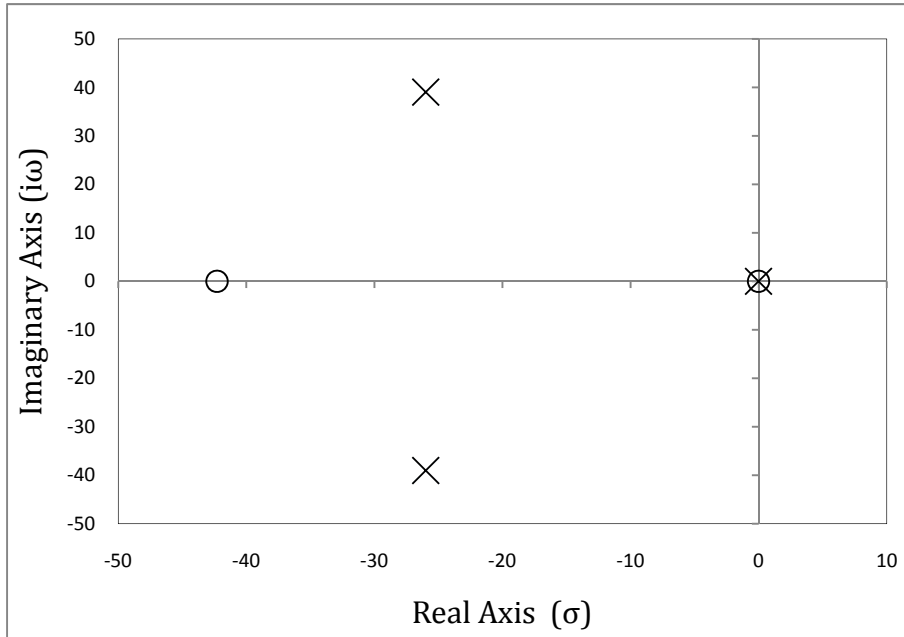


Figure 4-4: Pole zero plot of the closed loop transfer function. The poles are represented by an “x” and the zeros by “0” and the units are radians/second.

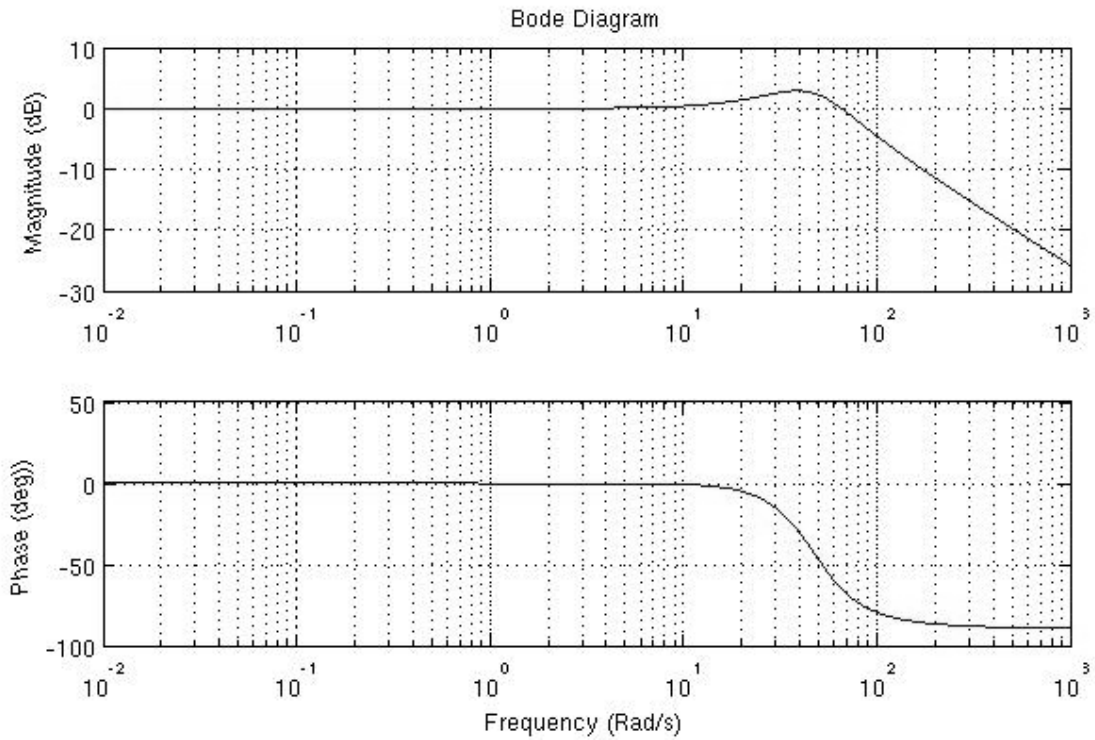


Figure 4-5: Bode diagram for model closed loop transfer function

4.7 Control Software

The control software for the seismometer was written in the graphical programming language LabVIEW by National Instruments running on a Dell Latitude 610 with Windows XP SP3. A block diagram and user interface of the program is found in Appendix B and C. The program developed for seismometer control and data acquisition is called “Seismometer_Control.VI.” This program compares the value of the voltage on the input channel of the National Instruments 6211 DAQ module with a user defined set point value. The difference is then routed to the PID subroutine or virtual instrument (VI) where the signal is scaled according to user defined PID parameters. The output of the PID sub VI is sent to the output channel on the DAQ where it is converted back to a voltage. This output voltage is then sent to the unity gain amplifier and ultimately to the voice coil actuator. The voltage out is limited to ± 3 V to prevent damage to the voice coil actuator.

The user interface has entry fields for the three PID parameters that can be changed during the operation of the seismometer. The sample time can be changed in 10 ms intervals from 10 ms to 100 ms and controls the time the PID sub VI updates the output value. Typically the sampling time should be 10 times smaller than the time constant of the system[28]. For this reason, the sampling time is usually set to 10ms. The interface also includes the path to file, a record data option, a process variable and output voltage display, and set point control.

The PID sub VI has an autotuning feature built into the module. Before autotuning can be performed, the process must be stable where the process variable is oscillating about the set point. The autotuning feature uses the Ziegler–Nichols method described in Section

4.5. The autotuning method is heuristic and assumes a first order system but may still be useful in loop tuning [28].

Data is written as a four-column text file to the specified file and path if the append button is pressed before the start of the data acquisition. The first column of the tab delimited data is the system elapsed time in seconds since January 1, 1904. The second column is the output voltage to the actuator, the third column is the process variable, which is proportional to the displacement of the proof mass, and the last column is the user defined set point.

5. OPERATION

Successful closed loop operation of both seismometers was accomplished. The electrical connections were made between the seismometer and the lock-in amplifier, National Instruments DAQ, and the unity gain operational amplifier. Each seismometer was tuned and the output was recorded to file.

The custom acrylic bell jars from Nevada Vacuum have not arrived at the time of this writing and are crucial for the proper operation of the seismometers. For the operation performed in this thesis, a single oversized glass bell jar was placed over the seismometer during tuning and operation. The oversized bell jar was too large to sit on the base plate of the seismometer, therefore the bottom edge rested on the three cables that lead to the seismometer. As a result, a one-centimeter gap was left around the bottom of the bell jar.

5.1 Tuning Procedure

The seismometer control user interface includes three PID parameters that can be adjusted during operation. Actual implementation of the PID algorithm in LabVIEW is slightly different than the ideal method described in 4.3 above. Here the PID parameters are K_c , T_i , and T_d . The controller output is described by [28]

$$V_{fb}(t) = K_c \left(v_e(t) + \frac{1}{T_i} \int_0^t v_e(\tau) d\tau + T_d K_d \frac{d}{dt} v_e(t) \right), \quad (4.15)$$

Where K_c is the controller gain, T_i is the integral time in minutes, and T_d is the derivative time in minutes. Therefore the actions of the proportional, integral, and derivative terms follow respectively

$$V_{fbp}(t) = K_c v_e(t)$$

$$V_{fbi}(t) = \frac{K_c}{T_i} \int_0^t v_e(\tau) d\tau \quad . \quad (4.16)$$

$$V_{fbi}(t) = K_c T_d \frac{d}{dt} v_e(t)$$

After the seismometer was leveled, the lock-in amplifier, power supply to the unity gain amplifier, and the seismometer control program were initialized. Next, the lock-in amplifier settings were entered. Table 5-1 lists important settings on the lock-in amplifier that were found to work well.

Table 5-1: Selected lock-in amplifier settings used in seismometer operation

Time constant	Sensitivity	Gain	Phase	Frequency
3 ms	500 μ V	1x	90 deg	17 KHz

The equilibrium position of the proof mass typically rests at one of the sides of the capacitor and not in the middle of the gap, despite careful leveling. This causes the initial value of the process variable to be far away from the set point.

First the K_c value was increased until the proof mass separated from the base capacitor. Typical values were around 0.005 or .01 but this depended on the initial leveling. Oscillations were present at this point. To reduce the oscillations, a large initial value of T_i (0.1) was used. The value of T_i was then gradually reduced until its contribution reduces or eliminated the offset. A proper T_i setting also reduced the oscillations. Then, ramp up of the K_c value while ramp down of the T_i value was performed until the process variable exhibited small oscillations about the set point.

When the process variable was stable and exhibiting little or no oscillations about the set point, the autotune feature was initiated. A screen showing the live time series of the

set point, process variable, and output voltage were all displayed. The live time series was also an aid in further manual tuning. The autotune feature estimates the noise level in the PV and then introduces step changes to the set point. If the process remains stable during the autotuning, the display returns parameters for K_c , T_i , and T_d . The new parameter can be entered back into the respective fields.

Stable operation about the set point was achieved with the PID values in table 5-2 where each seismometer had been given a numerical label. These values were determined empirically and do not uniquely represent a stable condition. In fact, it is thought that the seismometer response can be improved as discussed in Section 5.2.

Table 5-2: PID values for seismometer control

PID Values	Seismometer 1	Seismometer 2
K_c	.026	.056
T_i	.01	.02
T_d	.005	.003

5.2 Step Response

With the values for the PID constants in table 5-2 and the lock-in settings in table 5-1, stable closed loop operation of the seismometers was accomplished. While in stable operation, data was written to file for each seismometer. During the acquisition, a 0.5 v step change was given to the set point variable. Figure 5-1 is the response of each seismometer to the step change. Both seismometers exhibit very low deadtime at approximately 30 ms. The settling time for seismometer 1 is approximately one second while the second seismometer is closer to 0.5 seconds. Overshoot is also controlled to

about 20% for seismometer 1 and half that for seismometer 2. This is expected from the PID values listed in the table above.

When the PID parameters are adjusted for a faster rise time, the system exhibits instability when the loop is first closed. This is largely due to two factors. First, the starting value of the PV is very far from the set point. The large current sent to the voice coil actuator to bring the PV to the set point causes the LM675T operational amplifier to overheat. The amplifier will shut down when the temperature spikes to 170⁰ C or is sustained above 150⁰ C. A heat sink added to the amplifier has reduced but not eliminated the effect. Secondly, when PID parameters are adjusted for a faster rise time, the proof mass oscillates between the base capacitors. When the proof mass undergoes large oscillations, the squeeze-film damping discussed in Section 4.1 is no longer a good approximation and damping is significantly larger and nonlinear. Such aggressive PID parameters are only valid near the set point. This is addressed further in Section 6.1.

The output voltage is proportional to ground acceleration and is often the signal to analyze. The output voltage from the controller during the performed step function rose to just a few millivolts since the force sensitivity of the voice coil actuator is over 0.5 N/A. To resolve ground acceleration in this channel, the current to voltage ratio must be reduced. A possible solution is presented in Section 6.1.

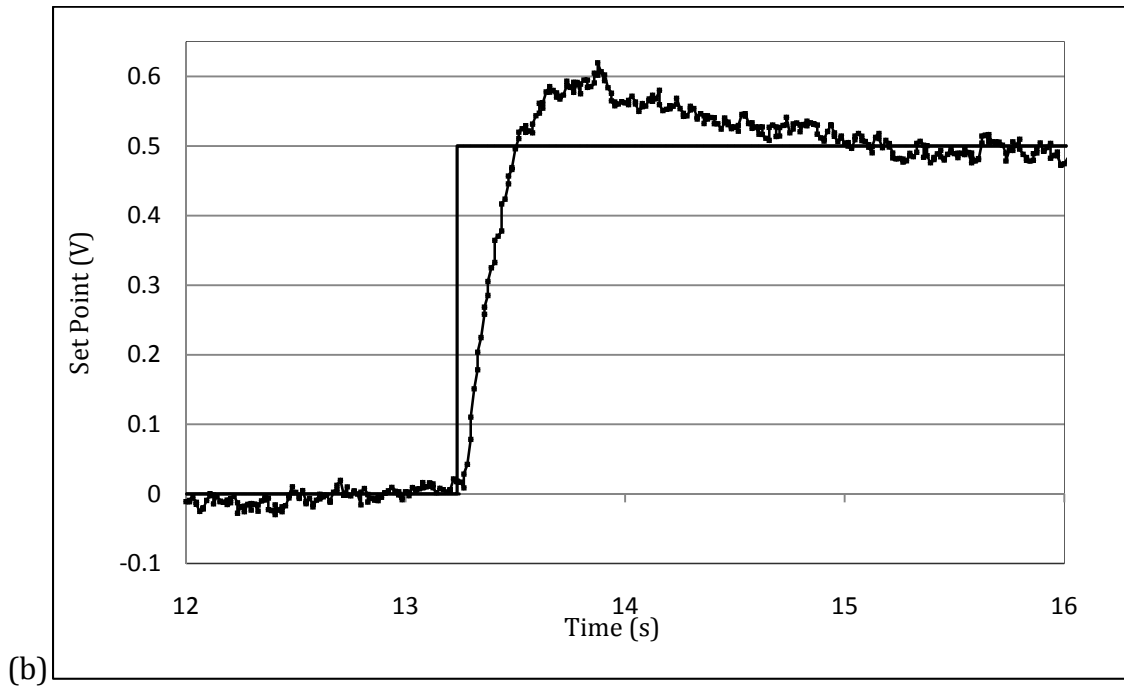
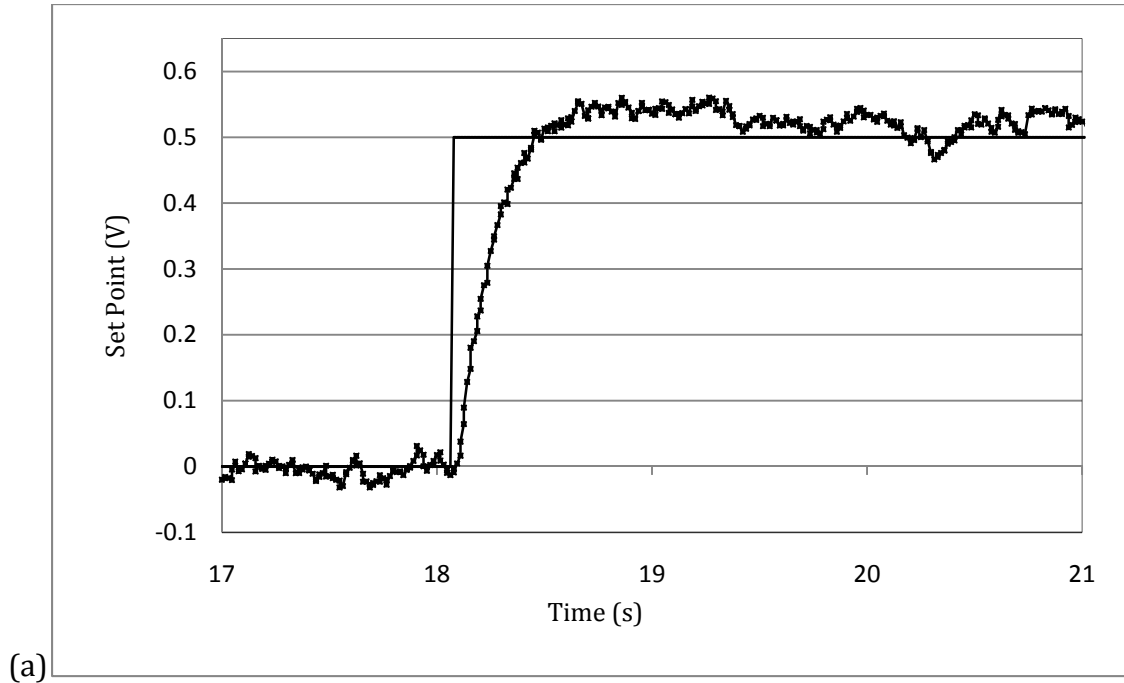


Figure 5-1: (a) Step response of seismometer 1; (b) step response of seismometer 2

6. CONCLUSION

Two identical broadband force balance seismometers were designed, fabricated, assembled, and operated in closed loop operation. A software program was written to control the feedback, change operating parameters, and write data to file during operation. An ideal model of the seismometers was developed in software and the performance of the model step response was compared with the actual step response of the seismometers. The settling time, overshoot, and deadtime of the seismometers were used as a metric for performance. The target settling time of 0.1 second was achieved in the software model. The actual model performance was between 0.5 seconds and approximately 1 second. Overshoot of the set point in the seismometer was better than the model and was limited to 20% in seismometer 1 and 10% in seismometer 2. The seismometers exhibit very little dead time at just 30 ms.

6.1 Recommendations for Further Development

The seismometers are fully operational but further work is needed before ground motion measurements can take place. Arguably the most important issue to be addressed is the level of the output signal to the voice coil actuator. The voltage from the DAQ required to supply the restoring force to the proof mass during the 0.5 V step change is a few tens of milliamps. Ideally, this signal is proportional to ground acceleration and is the signal that is often analyzed. During ground excitation this signal should be of order volts with clipping at 10 V. To achieve this, a series resistor could be placed in the voice coil circuit to reduce the current to voltage ratio. If the LM675T and the DAQ are limited to

± 10 V and the actuator is limited to 1.2 amps, a 4Ω resistance with 5 W power rating would be appropriate. In this configuration, a larger heat sink for the power amplifier with better thermal coupling would be required.

Another method of controlling the large response of the seismometers during initialization is set point ramping.

After a suitable signal level is obtained in the output, a calibration procedure should be performed. There are several ways of performing a calibration to correlate the output voltage to ground acceleration or velocity[5], [29]. Calibration methods include the use of shaker tables or comparing the output with that of a commercial seismometer that has been calibrated. Another method involves adding a known tilt to the seismometer by adjusting one of the legs or supplying an additional voltage to the voice coil actuator via separate circuit. After the calibration, noise measurements of the two seismometers can be made. Holcomb [30] describes a method where two seismometers operating simultaneously at the same site can be used to quantify the seismometer noise.

REFERENCES

1. Hannon, W.J., *Seismic Verification of a Comprehensive Test Ban*. Science, 1985. **227**(4684): p. 251-257.
2. Koketsu, K. and H. Miyake, *A seismological overview of long-period ground motion*. Journal of Seismolog, 2008. **12**(2): p. 133-143.
3. Abbott, R. and et al., *Seismic isolation for Advanced LIGO*. Classical and Quantum Gravity, 2002. **19**(7): p. 1591.
4. Safranek, J. *Orbit control at synchrotron light sources*. in *International Conference on Accelerator and Large Experimental Physics Control Systems*. 1999.
5. Wielandt, E., *Seismic sensors and their calibration*, in *New manual of seismological observatory practice*, P. Bormann, Editor. 2002, GeoForschungsZentrum Potsdam: Potsdam, Germany.
6. Abbott, R. and et al., *Seismic isolation enhancements for initial and Advanced LIGO*. Classical and Quantum Gravity, 2004. **21**(5): p. S915.
7. Luiten, A.N., et al., *Ground tilt seismic spectrum measured with a new high sensitivity rotational accelerometer*. Review of Scientific Instruments, 1997. **68**(4): p. 1889-1893.
8. Speake, C.C. and D.B. Newell, *The design and application of a novel high-frequency tiltmeter*. Review of Scientific Instruments, 1990. **61**(5): p. 1500-1503.
9. Winterflood, J., et al., *Tilt sensor and servo control system for gravitational wave detection*. Class. Quantum Grav., 2002. **19**: p. 1723-1729.
10. Lantz, B., et al., *Review: Requirements for a Ground Rotation Sensor to Improve Advanced LIGO*. Bulletin of the Seismological Society of America, 2009. **99**(2B): p. 980-989.
11. Bertolini, A., et al., *Readout system and predicted performance of a low-noise low-frequency horizontal accelerometer*. Nuclear Instruments and Methods in Physics Research Section A: Accelerators, Spectrometers, Detectors and Associated Equipment, 2006. **564**(1): p. 579-586.
12. Peterson, J., *Observations and modeling of seismic background noise*. 1993, US Geol. surv.: Albuquerque.

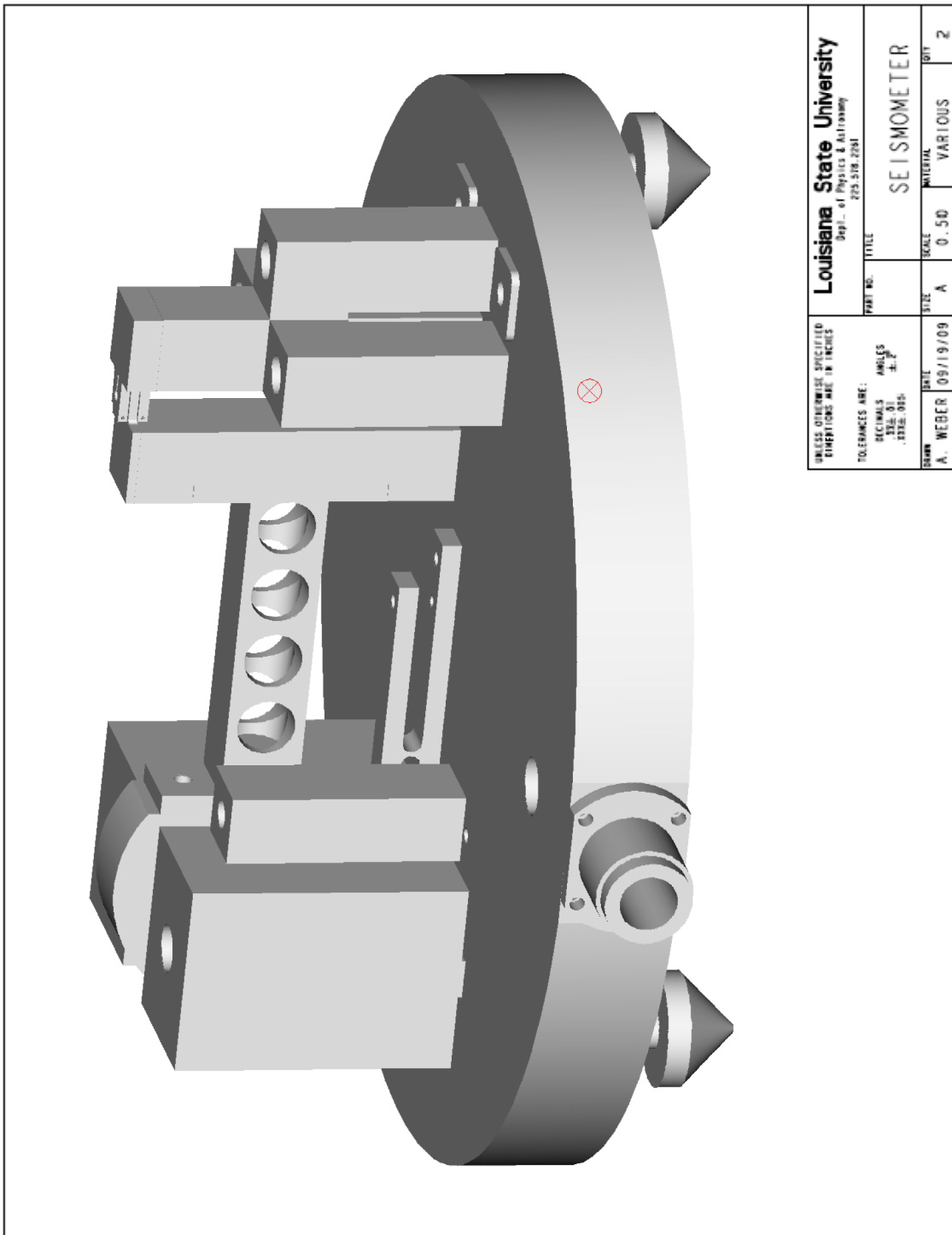
13. Halliday, B.S., *Cleaning materials and components for vacuum use*. Vacuum, 1987. **37**(8-9): p. 587-591.
14. Traeger, H., *Considerations in the application of flexural pivots*. Automatic Control Data Systems Engineering, 1962. **17**(4).
15. <http://www.flexpivots.com>.
16. Usher, M.J., *Developments in seismometry*. Journal of Physics E: Scientific Instruments, 1973. **6**(6): p. 501-507.
17. Jones, R.V. and J.C.S. Richards, *The design and some applications of sensitive capacitance micrometers*. Journal of Physics E: Scientific Instruments, 1973. **6**(7): p. 589.
18. Bao, M., et al., *Effects of electrostatic forces generated by the driving signal on capacitive sensing devices*. Sensors and Actuators A: Physical, 2000. **84**(3): p. 213-219.
19. *Model SR830 DSP Lock-In Amplifier*. Revision 2.3, 2006, Stanford Research Systems, 1290-D Reamwood Avenue Sunnyvale, CA 94089.
20. *LM675 Power Operational Amplifier manual*. 1999 [cited 2009; Available from: <http://www.national.com>].
21. <http://www.beikimco.com>.
22. Wielandt, E. and G. Streckeisen, *The leaf-spring seismometer: Design and performance* Bulletin of the Seismological Society of America, 1982. **72**(6A): p. 2349-2367.
23. Block, B. and R.D. Moore, *Measurements in the Earth Mode Frequency Range by an Electrostatic Sensing and Feedback Gravimeter*. J. Geophys. Res., 1966. **71**(18).
24. Bao, M. and H. Yang, *Squeeze film air damping in MEMS*. Sensors and Actuators A: Physical, 2007. **136**(1): p. 3-27.
25. Dorf, R.C. and R.H. Bishop, *Modern Control Systems*. 11 ed. 2007: Prentice Hall.
26. Ziegler, J.G. and N.B. Nichols, *Optimum settings for automatic controllers*. Trans. ASME, 1942. **65**: p. 433-444.
27. Scherbaum, F., *Of Poles and Zeros: Fundamentals of Digital Seismology*. 2 ed. 2007: Springer.
28. *LabVIEW PID Control Toolkit User Manual*. 2008 [cited 2009; Available from: <http://www.ni.com/>].

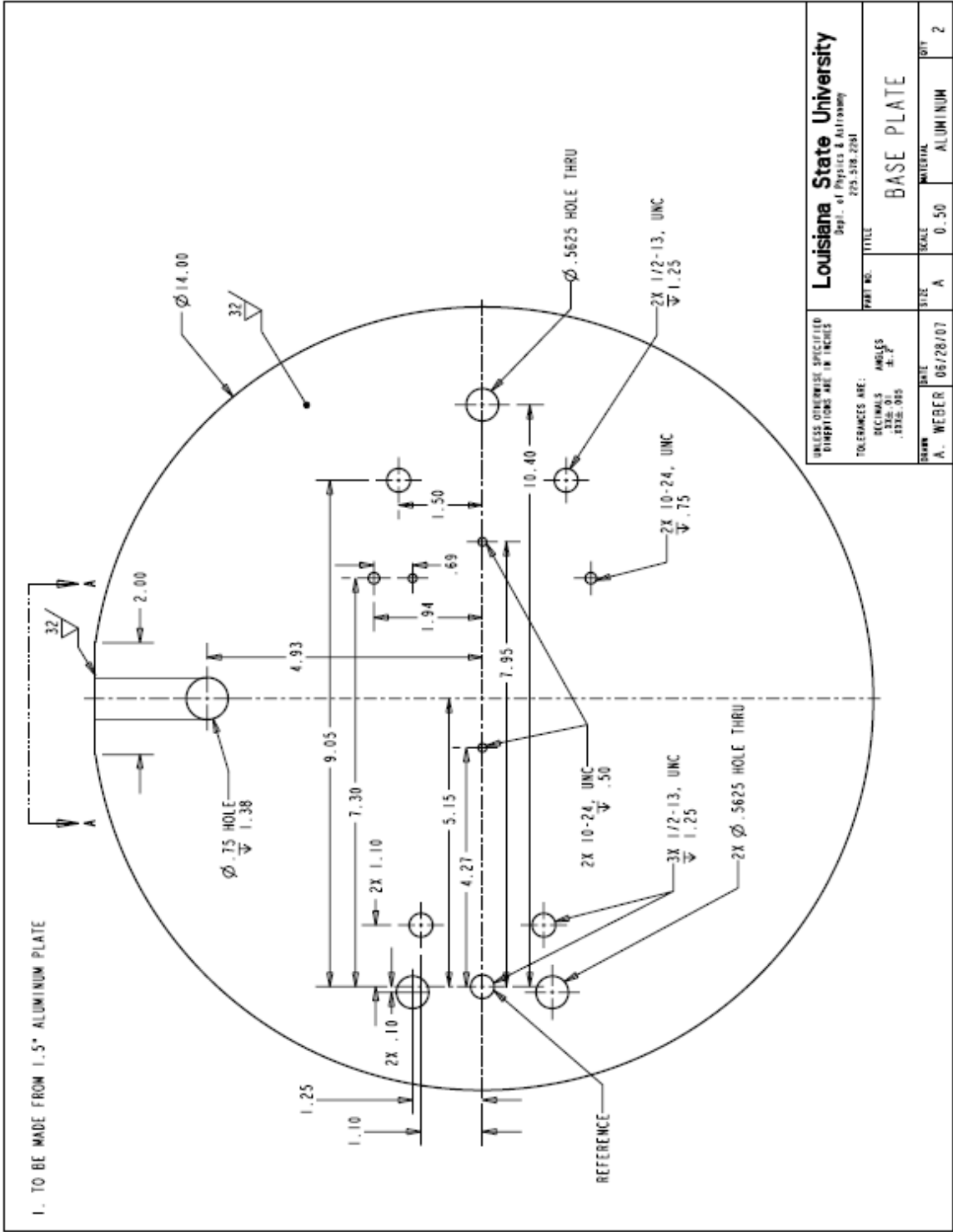
29. Mitronovas, W., *Temperature effects on long-period seismographs: an accurate method to determine the transfer function* Bulletin of the Seismological Society of America, 1976. **66**(4): p. 1405-1412.
30. Holcomb, G.L., *A direct method for calculating instrument noise levels in side-by-side seismometer evaluations*, U.S.D.o.t.I.G. Survey, Editor. 1989.

APPENDICES

A. Mechanical Drawings

Drawings in Appendix A are not to scale indicated in drawings.





Louisiana State University
Dept. of Physics & Astronomy
225-518-2281

UNLESS OTHERWISE SPECIFIED
DIMENSIONS ARE IN INCHES

TOLEANCES ARE:
DECIMALS
32±.01
ANGLES
±.2°
RHOSES
±.015

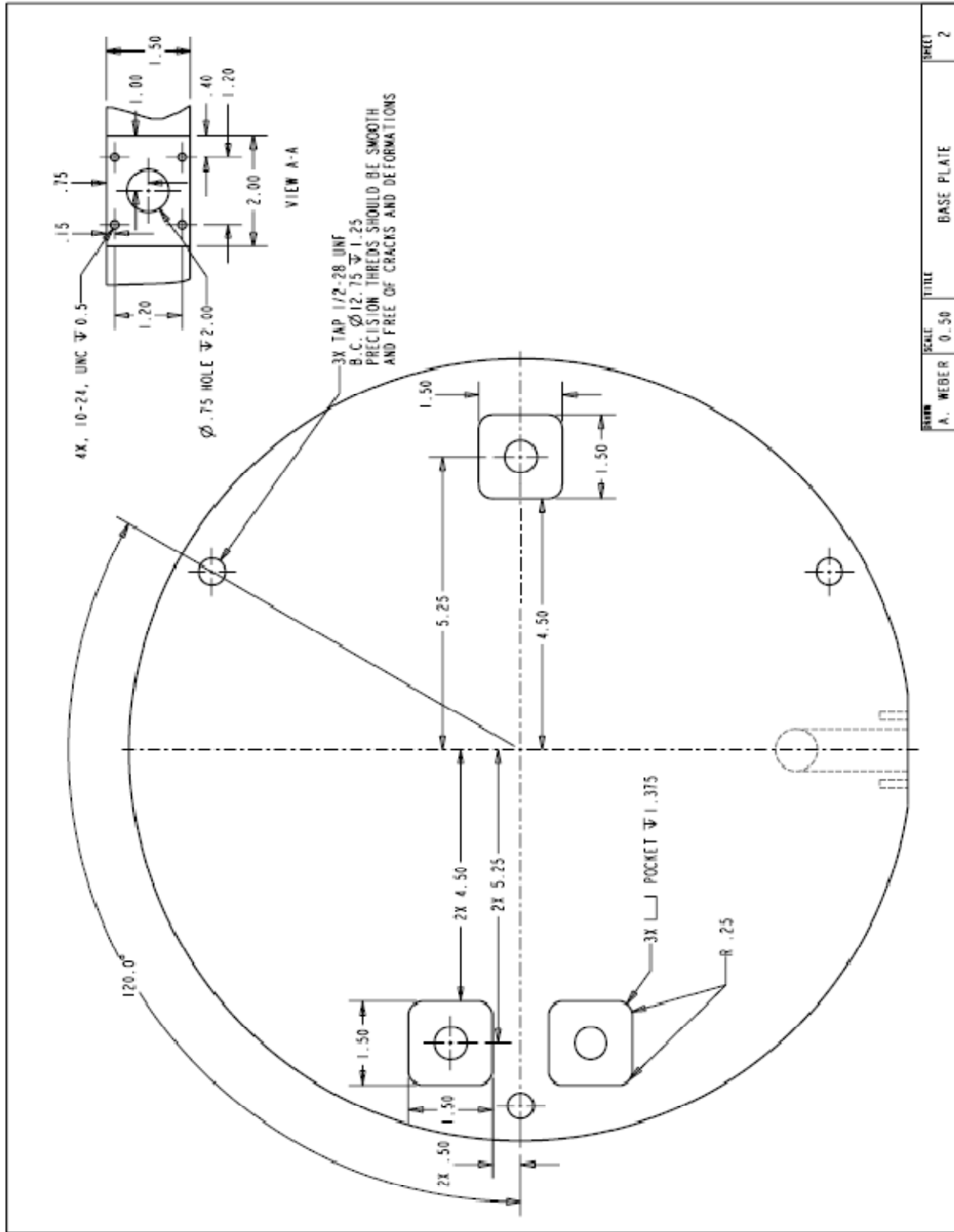
DATE 06/28/07

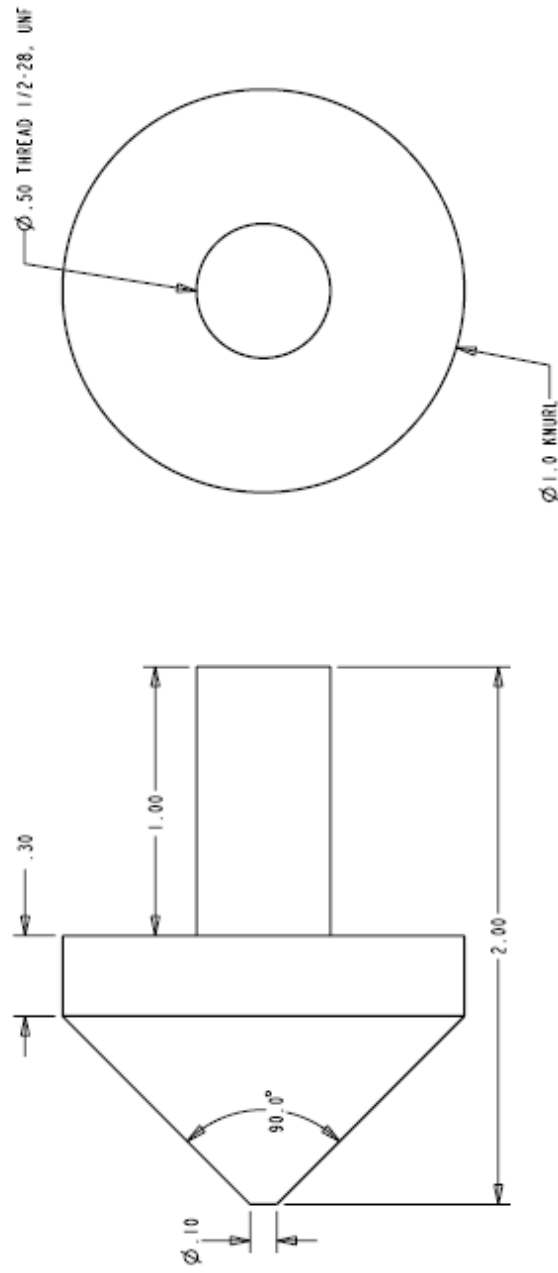
SCALE 0.50

MATERIAL ALUMINUM

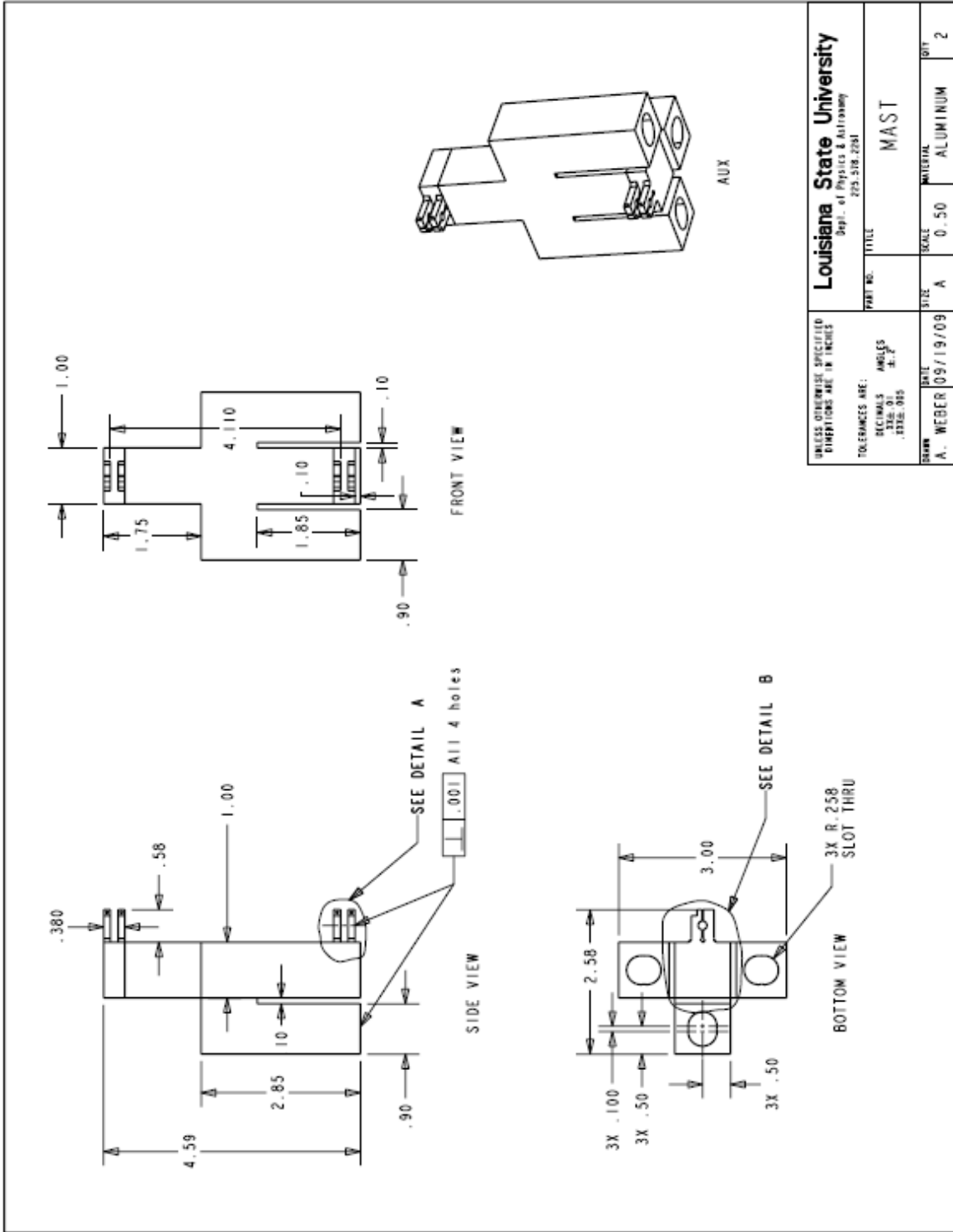
DRW A. WEBER

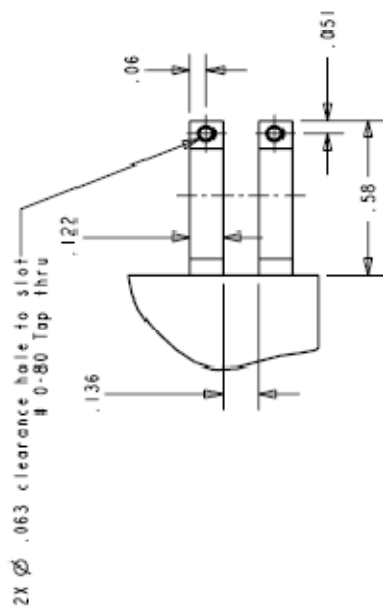
QTY 2



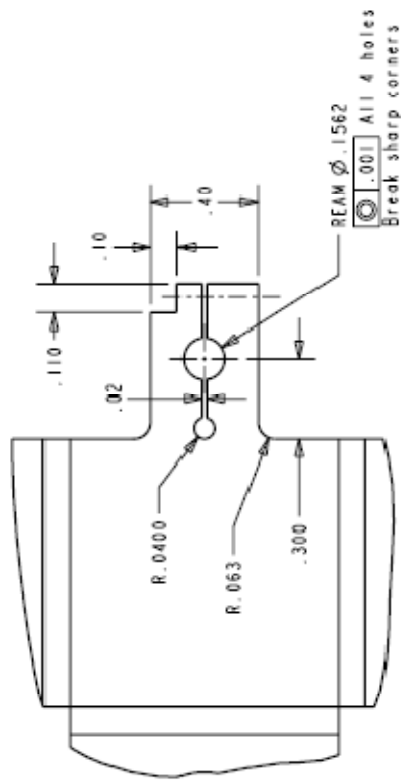


UNLESS OTHERWISE SPECIFIED DIMENSIONS ARE IN INCHES		Louisiana State University Dept. of Physics & Astronomy 725-518-2781	
TOLERANCES ARE:	DECIMALS	TITLE	FOOT
	FRACTIONS	PART NO.	
	ANGLES	DATE	SCALE
	±.01	A. WEBER 09/19/09	A 2.00
	±.015	SIZE	MATERIAL
DRN		6	BRASS



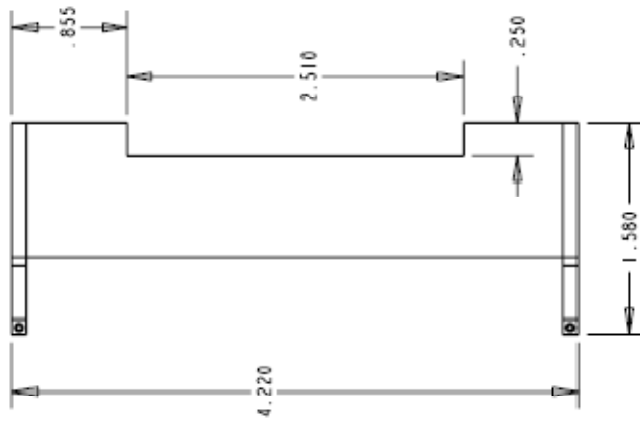
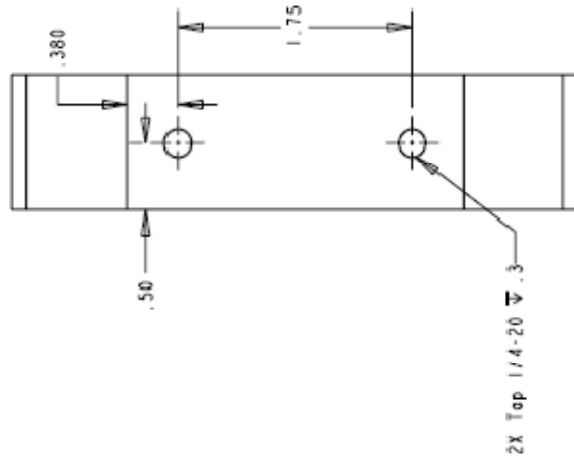


DETAIL A
SCALE 2.000

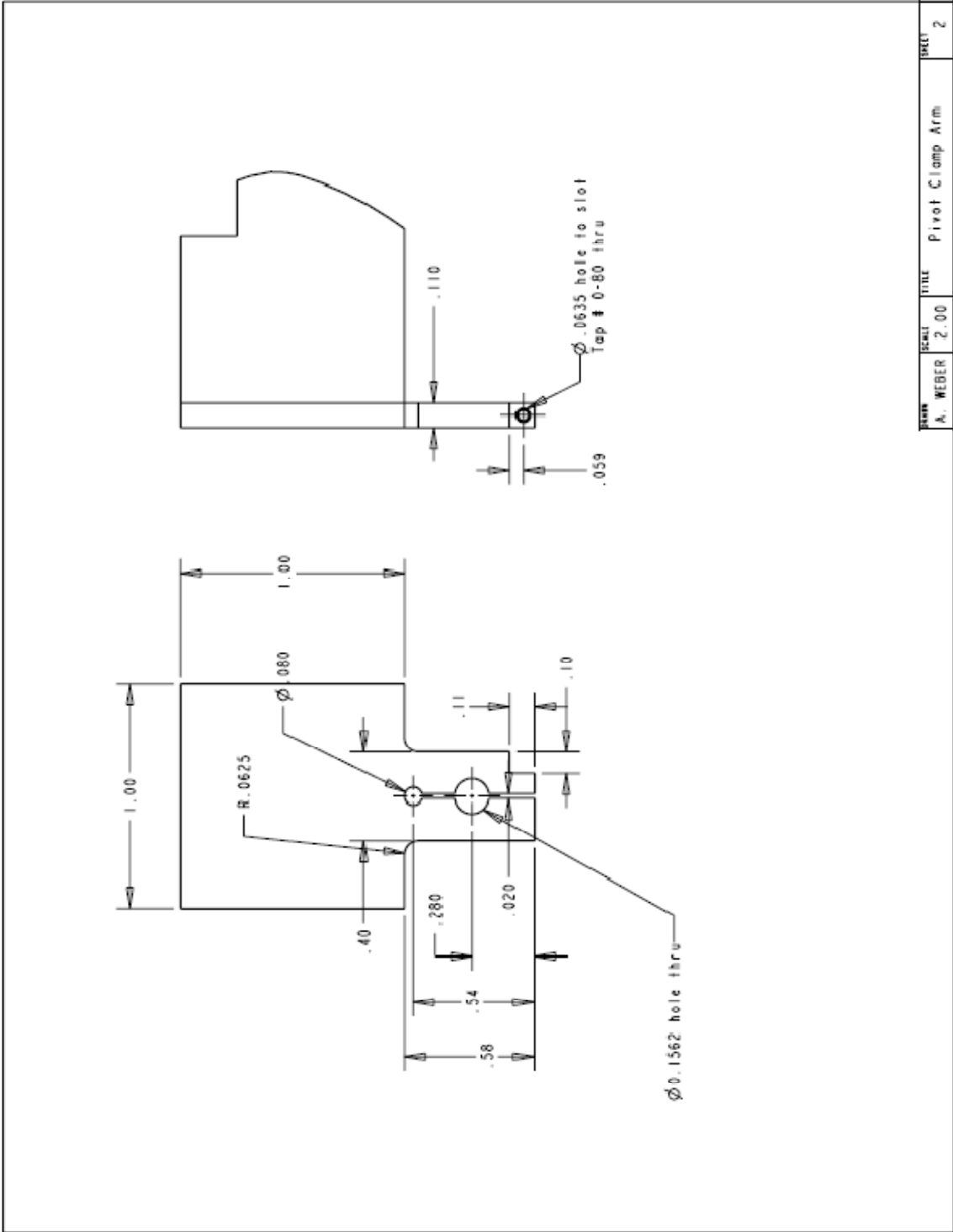


DETAIL B
SCALE 2.000

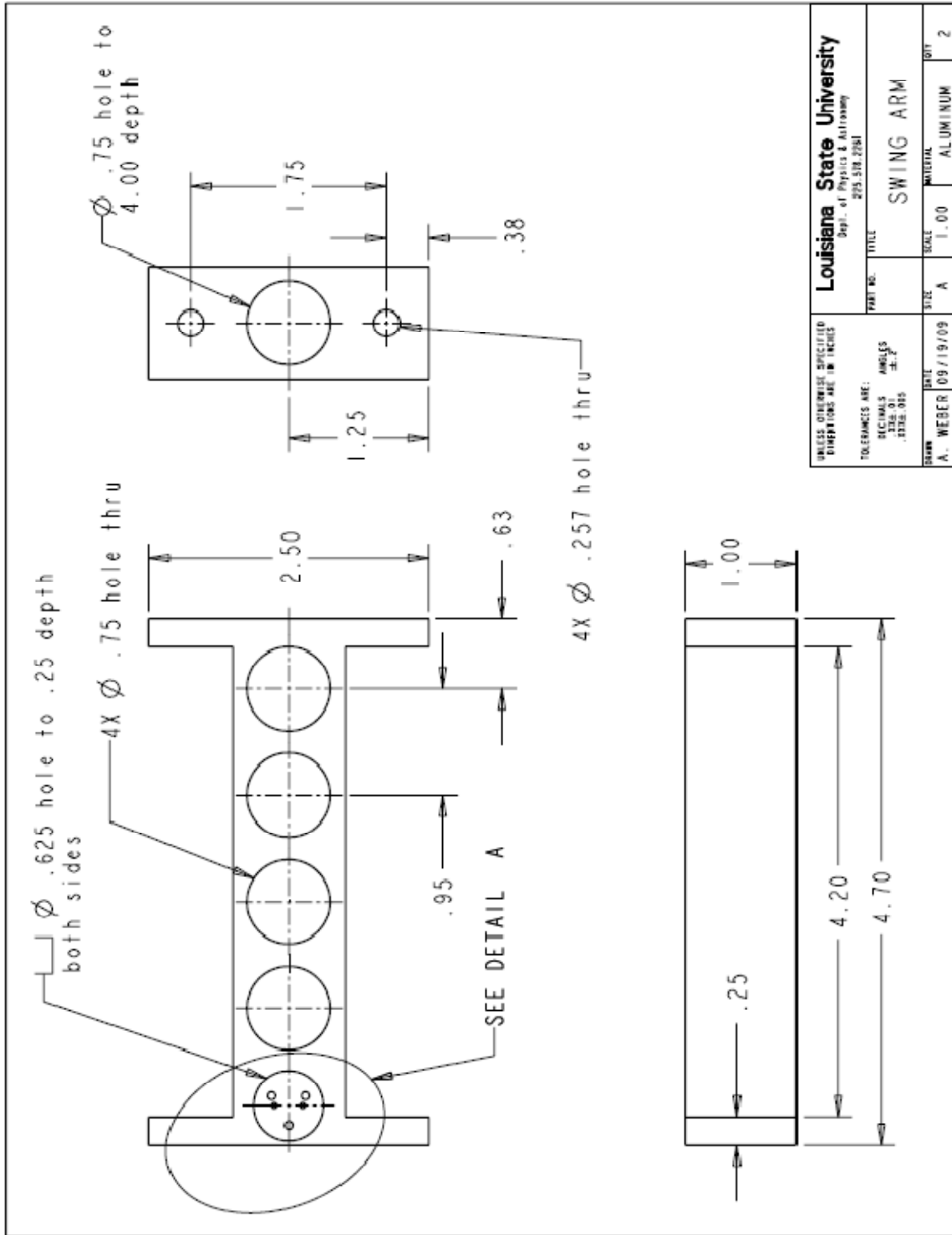
DRWN	SCALE	TITLE	SHEET
A. WEBER	2.00	MAST	2



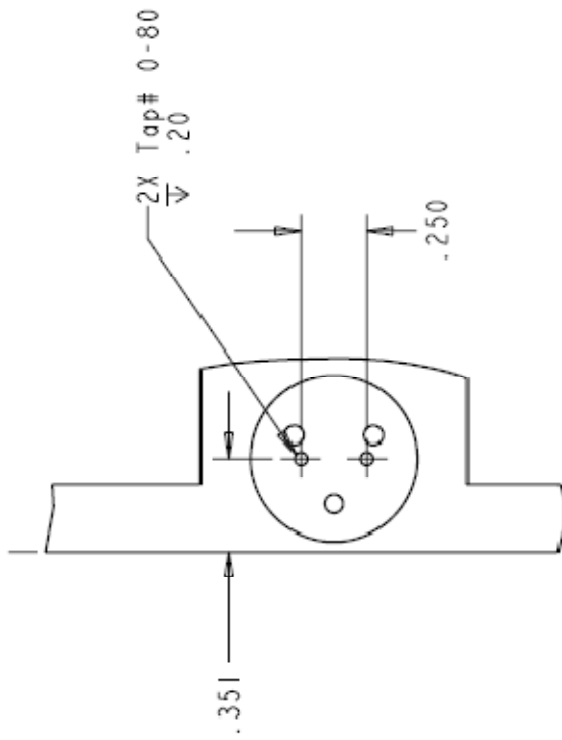
UNLESS OTHERWISE SPECIFIED DIMENSIONS ARE IN INCHES		PART NO.		TITLE	
TOLERANCES ARE: DECIMALS FRACTIONS ANGLES HOLE DIA. DRAUGHTS		DRAWN A. WIEGER		DATE 09/19/09	
LOUISIANA STATE UNIVERSITY Dept. of Physics & Astronomy 225 518 2281		SIZE A		SCALE 1:00	
		MATERIAL ALUMINUM		QTY 2	



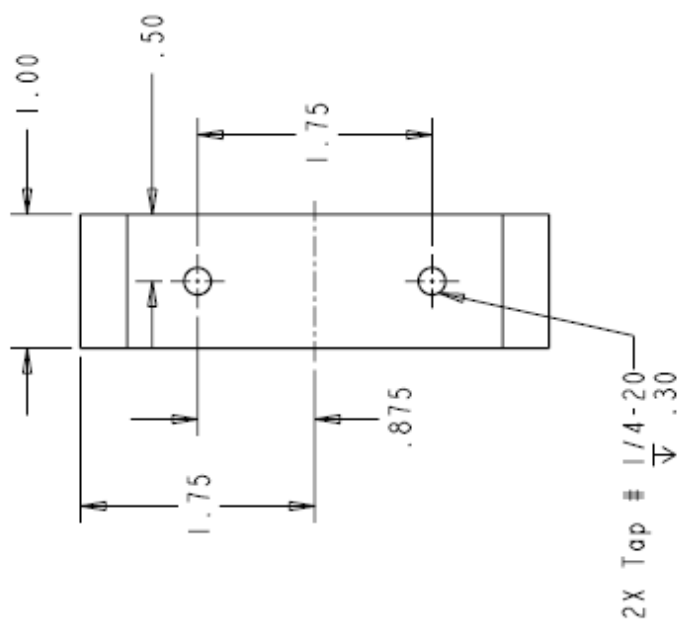
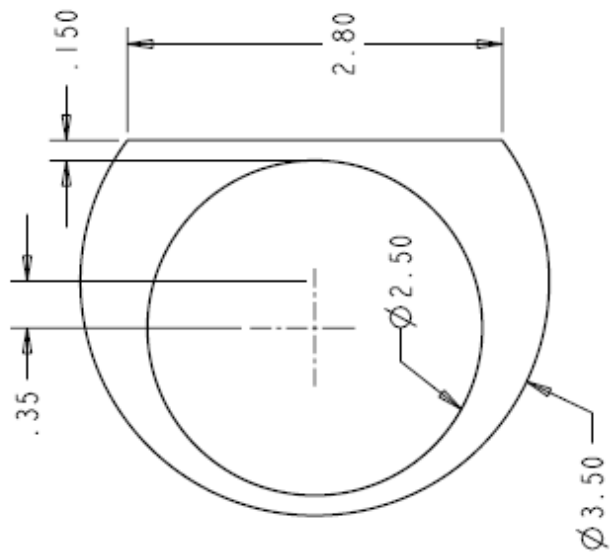
DESIGNER	SCALE	TITLE	SHEET
A. WEBER	2.00	Pivot Clamp Arm	2



Louisiana State University Dept. of Physics & Astronomy 225 518 2281		PART NO. TITLE	
DRAWN A. WEBER	DATE 09/19/09	SIZE A	SCALE 1:00
MATERIAL ALUMINUM		QTY 2	



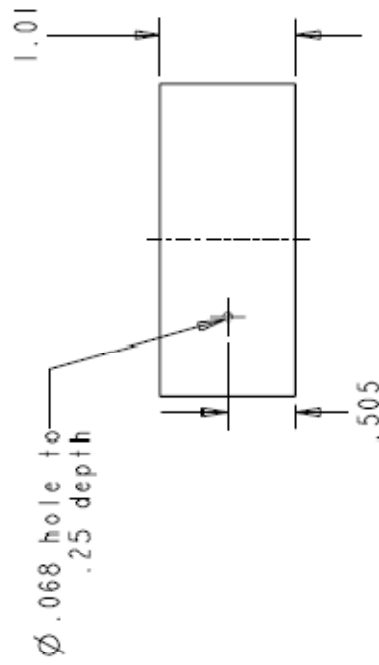
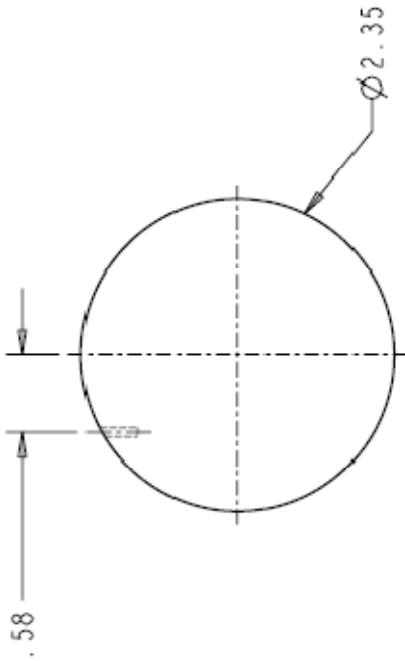
DESIGNER	SCALE	TITLE	SHEET
A. WEBER	2	SWING ARM	2/2



2X Top # 1/4-20
 ∇ .30

UNLESS OTHERWISE SPECIFIED DIMENSIONS ARE IN INCHES		Louisiana State University Dept. of Physics & Astronomy 225-518-2261	
TOLERANCES ARE:	DECIMALS	TITLE	PART NO.
	ANGLES		
	SIZE OF		
	TYPE OF		
	FINISH		
DRAWN	DATE	SITE	SCALE
A. WEBER	09/19/09	A	1.00
		MATERIAL	QUANTITY
		ALUMINUM	2

COPPER WIRE TO BE BRAZED INTO HOLE



UNLESS OTHERWISE SPECIFIED
DIMENSIONS ARE IN INCHES

TOLERANCES ARE:
DECIMALS ANGLES
FRACTIONS
.002, .015 .5, .2

DRAWN A. WEBER DATE 09/19/09

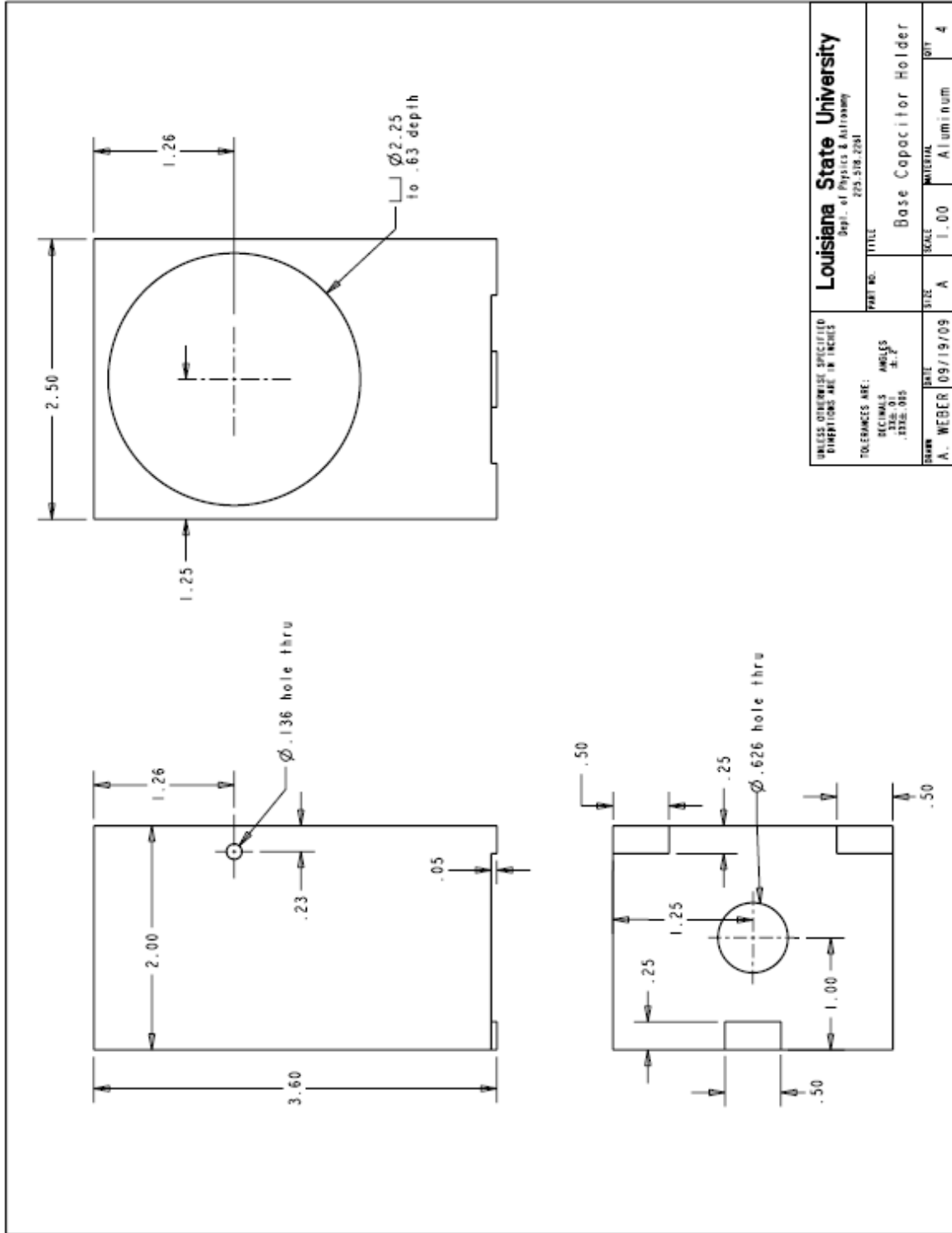
ALLEGRO GRAVITY EXPERIMENT GROUP
139 Dept. of Physics & Astronomy
225-516-3693

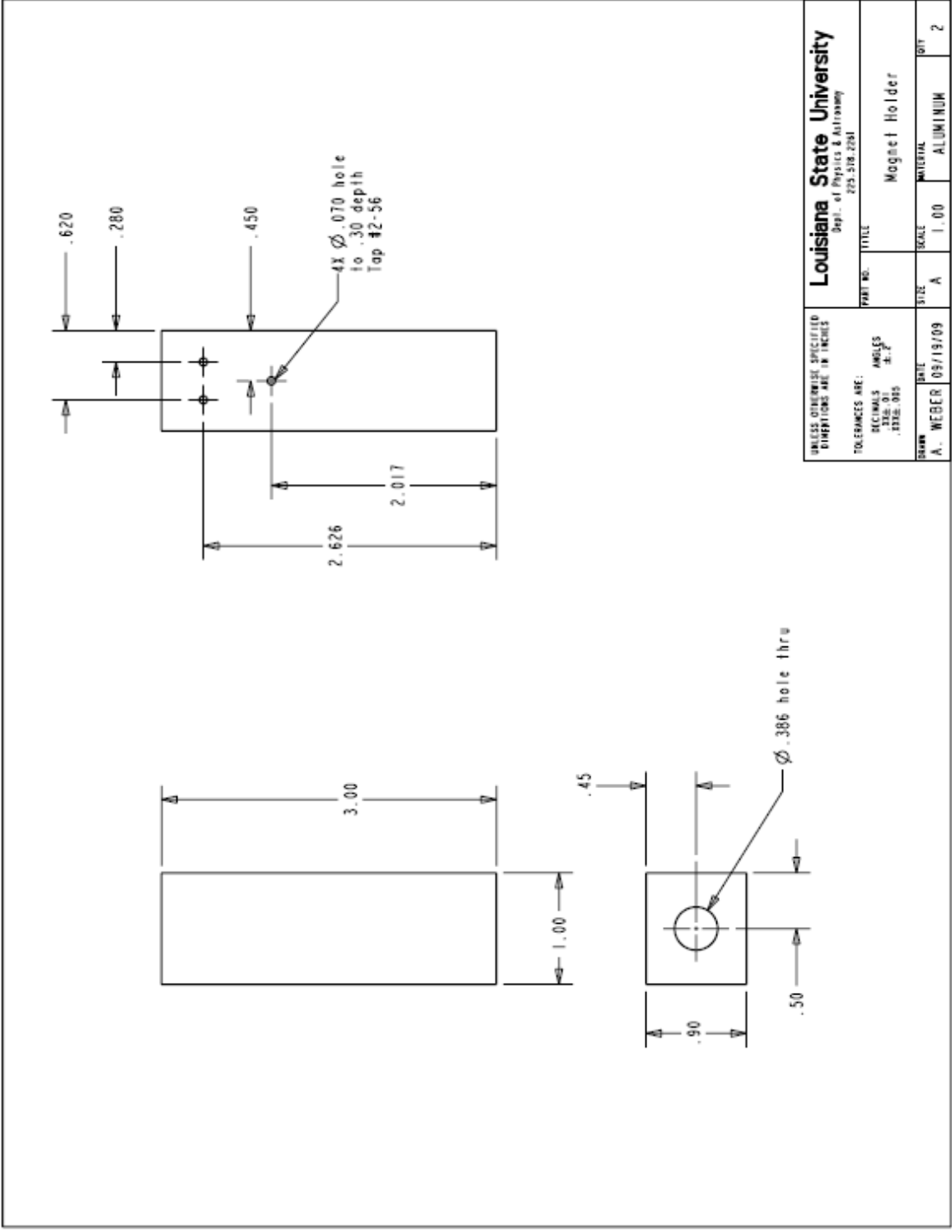
PART NO. TITLE

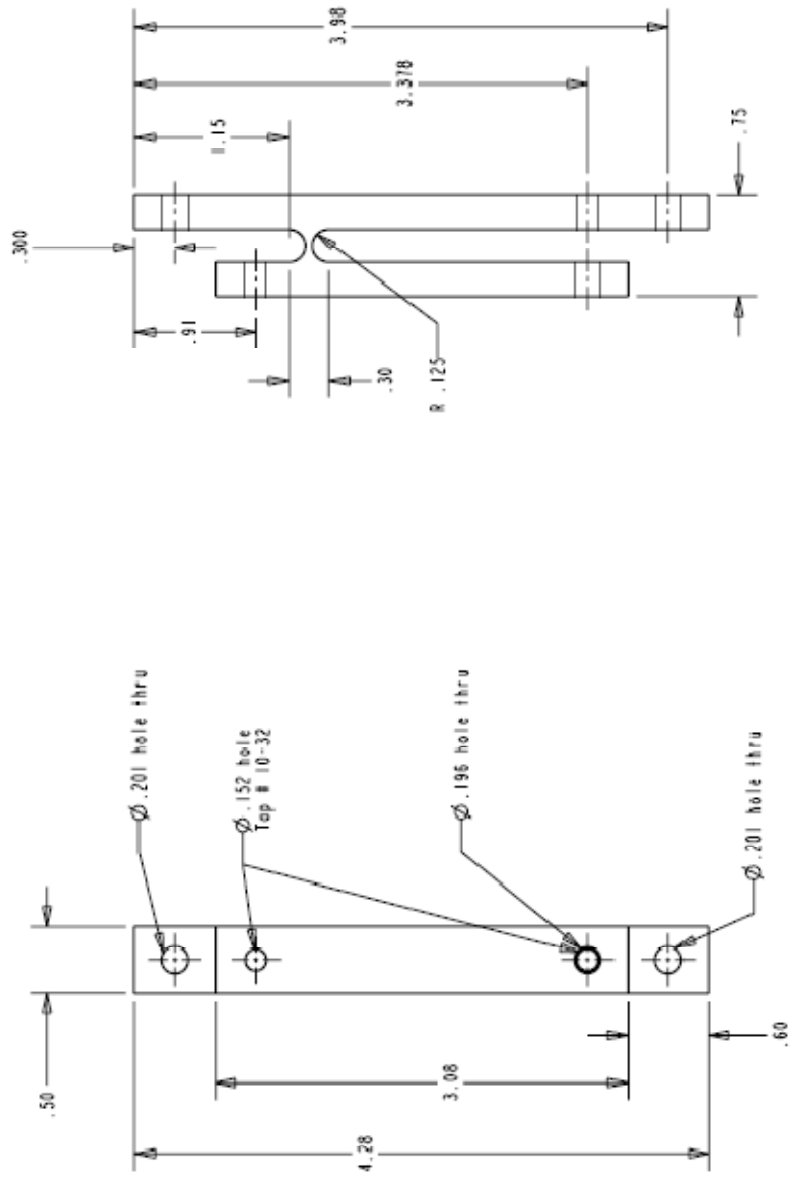
SIZE SCALE MATERIAL QTY

A 1.00 COPPER 2

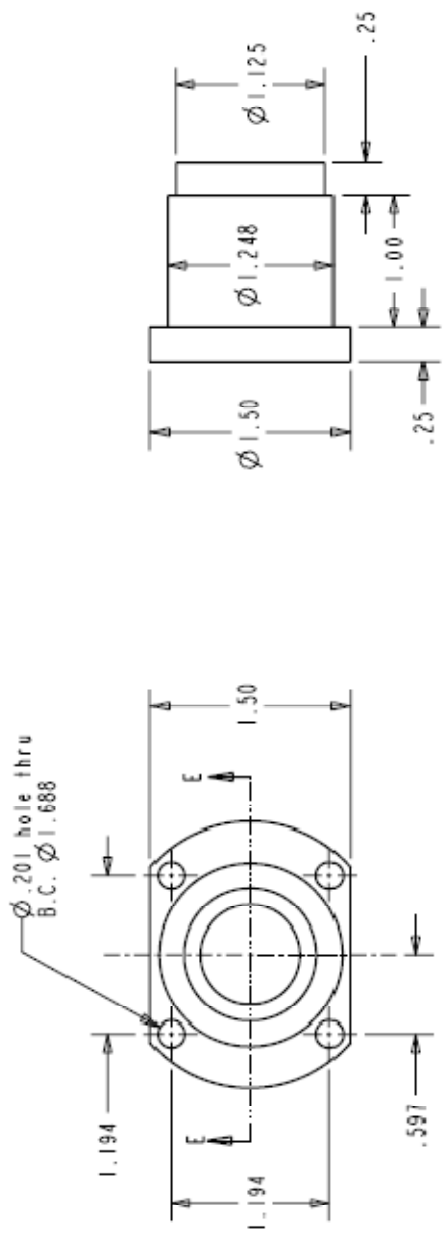
Proof Mass







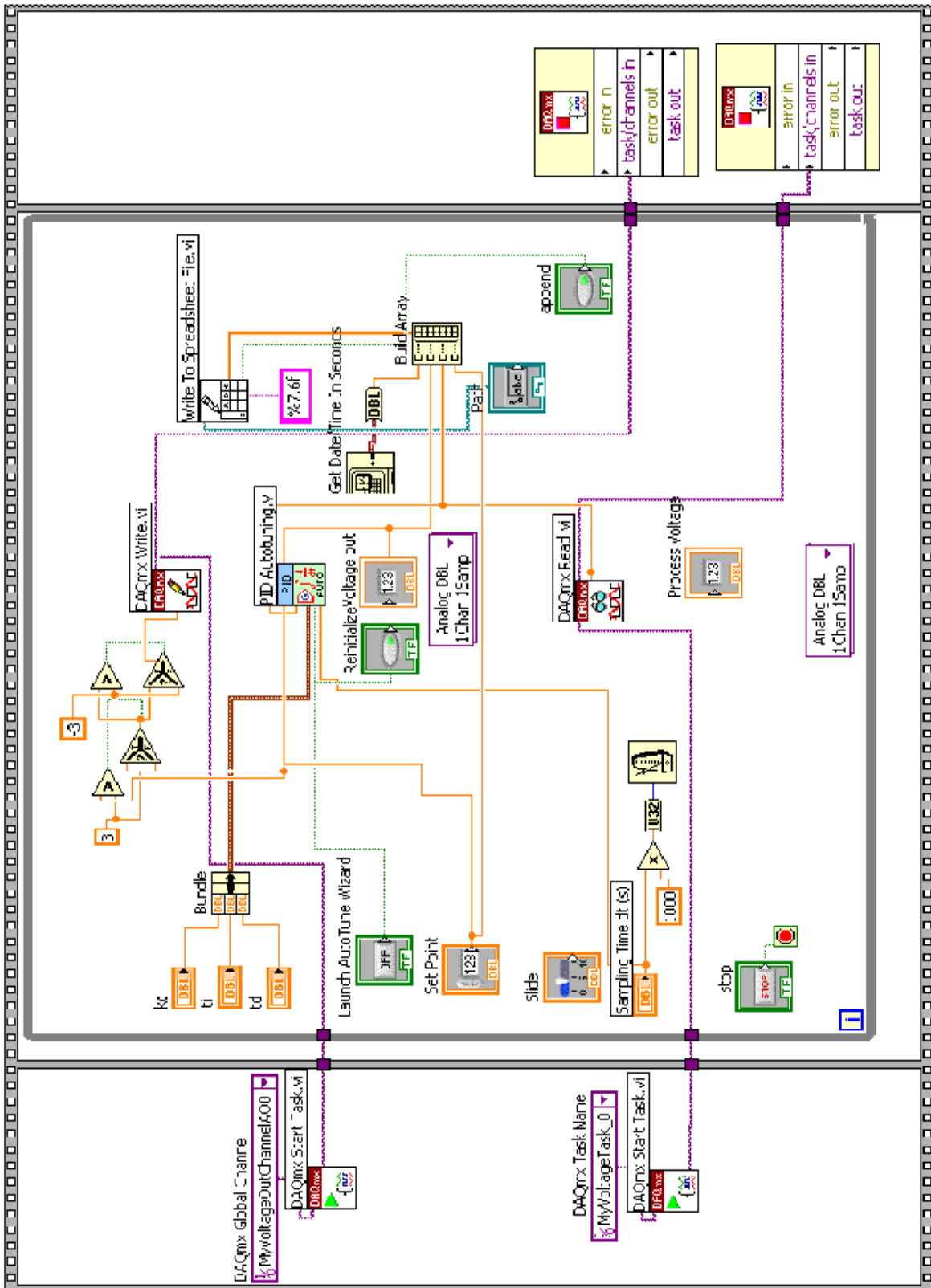
UNLESS OTHERWISE SPECIFIED DIMENSIONS ARE IN INCHES		PART NO. TITLE	
TOLERANCES ARE: DECIMALS ANGLES FRACTIONS HOLE DIA.		LIFTER	
DRAWN A. WEBER	DATE 09/19/09	SIZE A	SCALE 1:1.00
		MATERIAL ALUMINUM	QTY 2



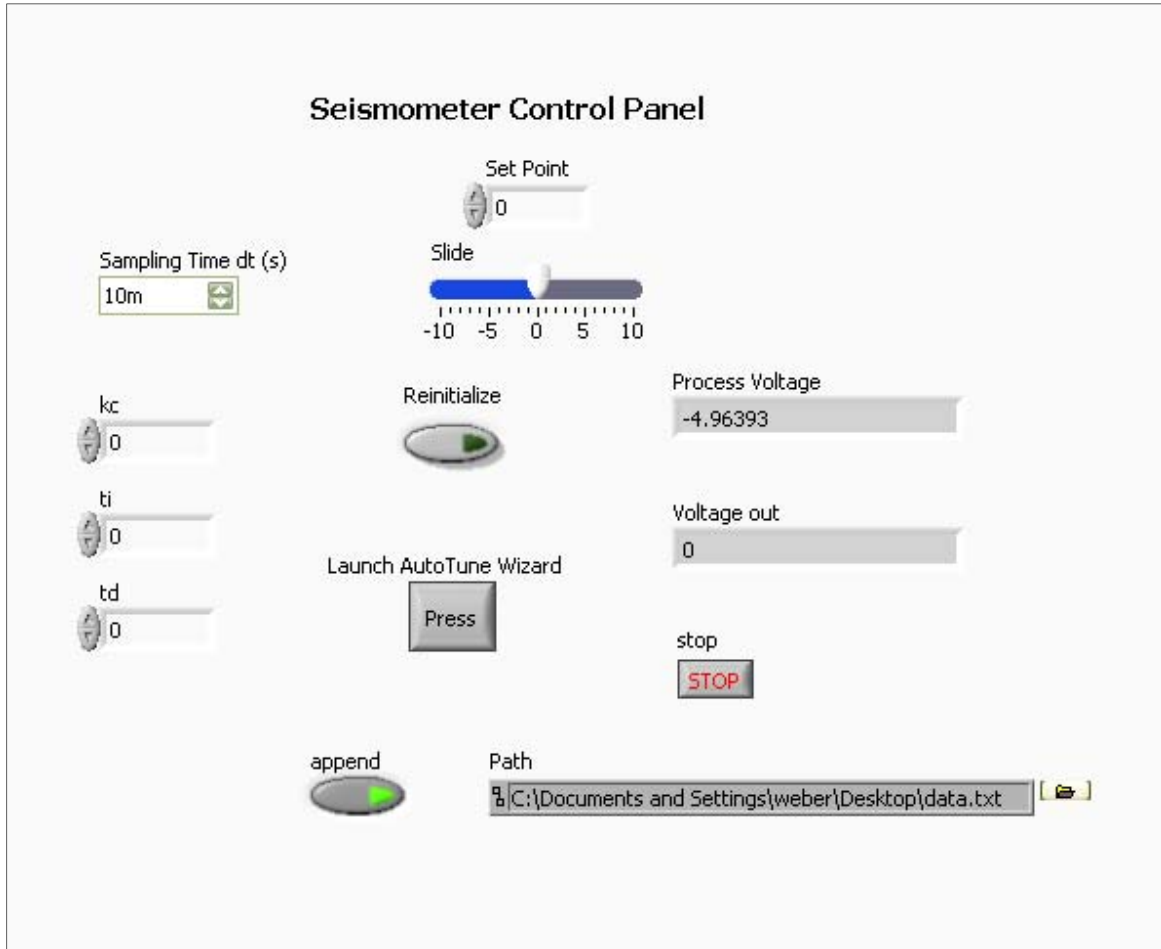
UNLESS OTHERWISE SPECIFIED DIMENSIONS ARE IN INCHES		TITLE	
TOLERANCES ARE:		PART NO.	
DECIMALS	ANGLES	Louisiana State University	
.005	.005	Dept. of Physics & Astronomy	
.010	.010	225-518-2261	
DRAWN		SCALE	TITLE
A. WEBER	05/19/09	A	PUMPOUT FLANGE
DATE		SCALE	MATERIAL
05/19/09		1:00	BRASS
DRAWN		SIZE	QTY
05/19/09		A	2

SECTION E-E

B. Seismometer_Control.vi Block Diagram



C. Seismometer_Control.vi User Interface



VITA

Andrew Weber was born in Anchorage Alaska in 1978 but moved shortly after. He spent the majority of his early years near Baltimore, Maryland where he would develop his interests in science in junior high and high school. His strong interests in science lead him to pursue his Bachelor of Science at the University of Maryland studying physics. During his time at University of Maryland, he was fortunate to work under the General Relativity Experiment group where he was able to participate in a wide range of experimental projects. His passion for experimental physics solidified during this time and he set his sights on graduate school. After graduating from the University of Maryland with a Bachelor of Science, Andrew Weber would ultimately choose to attend graduate school at Louisiana State University after close collaboration with the Allegro Group. He joined the Allegro Group under Professor Warren Johnson and continued his research in experimental gravitation for the remainder of the group's existence. Andrew continued to write his thesis under the guidance of Professor Warren Johnson for partial completion of the Master of Science degree.